

CHALMERS



Development of small scale hybrid wheel loader test platform

Master's Thesis in the Master's Programmes Electric Power Engineering and Systems, Control and Mechatronics

PER BJÖRE DAHL AND RICKARD NILSSON

Departments of Energy and Environment and Signals and Systems
Divisions of Electric Power Engineering and Automatic control, Automation & Mechatronics

CHALMERS UNIVERSITY OF TECHNOLOGY

Göteborg, Sweden 2012

Master's thesis EX035/2012

MASTER'S THESIS EX035/2012

Development of small scale hybrid wheel loader test platform

Master's Thesis in the Master's programmes Electric Power Engineering and
Systems, Control and Mechatronics

PER BJÖRE DAHL, RICKARD NILSSON

Departments of Energy and Environment and Signals and Systems
*Divisions of Electric Power Engineering and Automatic control, Automation &
Mechatronics*

CHALMERS UNIVERSITY OF TECHNOLOGY

Göteborg, Sweden 2012

Development of small scale hybrid wheel loader test platform

PER BJÖRE DAHL, RICKARD NILSSON

© Per Björe Dahl, Rickard Nilsson 2012

Master's Thesis 2012: EX035/2012

ISSN 1652-8557

Departments of Energy and Environment and Signals and Systems

Divisions of Electric Power Engineering and Automatic control, Automation & Mechatronics

Chalmers University of Technology

SE-412 96 Göteborg

Sweden

Telephone: + 46 (0)31-772 1000

Departments of Energy and Environment and Signals and Systems Göteborg, Sweden
2012

Development of small scale hybrid wheel loader test platform

Master's Thesis in the Master's Program Electric Power Engineering and Systems,
Control & Mechatronics

Per Björe Dahl, Rickard Nilsson

Departments of Energy and Environment and Signals and Systems

Divisions of Electric Power Engineering and Automatic control, Automation &
Mechatronics

Chalmers University of Technology

ABSTRACT

For construction equipment in general fuel efficiency is one of the most critical product attributes. Pure fuel economy improvements from the engines are extremely expensive to develop. This creates an incitement for development of hybrid technology. This thesis was done in corporation with CPAC Systems in Gothenburg, Sweden.

With regenerative braking, the energy that is normally transferred into heat during braking can be stored in a battery or a super capacitor and the stored energy can later be used for propulsion. However the regenerative braking also affects the vehicle dynamics and the driver's interpretation of the brake pedal which demands for a physical test platform for testing. In this thesis a test platform for testing of concepts was developed and built and a brake blending system was developed and tested on the test platform.

The test platform was built in small scale compared to a full wheel loader with an articulated rideable lawn mower as base. A small scale test platform has the benefits of fast and easy testing and much lower cost compared to a full scale wheel loader. The test platform is equipped with individual wheel motors and a mechanical brake system based on brakes from a motorcycle.

The first step in the development of the control system for the test platform was to make Simulink models for the components in the test platform. Models for the overall vehicle, the brakes and the electrical motors were developed. From the models a control strategy was developed to control the requested torque to the electric motors and the requested brake pressure to the brakes from the driver's inputs. The control strategy was developed in Simulink and from Simulink C-code was automatically generated by the code generation tool TargetLink. All testing including testing of the brake blending system was performed on the test platform.

The result of this thesis is a test platform that is built to emulate a small scale hybrid wheel loader. The test platform is expandable and can be used to test other concepts, for example steer-by-wire. The other result of the thesis is a brake blending system that is combining electrical and mechanical braking with good pedal feeling, no wheel lock and high energy regeneration.

Key words: Regenerative braking, brake blending, construction equipment, earth moving machinery, electric vehicle, brake system

Contents

ABSTRACT	I
CONTENTS	I
PREFACE	IV
NOTATIONS	V
1 INTRODUCTION	1
1.1 Background	1
1.2 Problem definition	1
1.3 Objectives	1
1.4 Method	2
1.5 Limitations	2
2 SYSTEM OVERVIEW	3
2.1 Overall system	3
2.1.1 Parallel hybrids	3
2.1.2 Serial Hybrids	3
2.1.3 Wheel loader hybrid concept	3
2.2 Electric motors	5
2.2.1 Construction	5
2.2.2 Operation	6
2.2.3 Mathematical model and dq representation	7
2.2.4 Control of PMSM	10
2.3 Brake system	11
2.3.1 Heat dependent dynamics	11
2.3.2 Limits, transients in applying brakes	12
2.3.3 Regenerative brake controller	13
2.4 Controller	13
3 IMPLEMENTATION OF MODELS	14
3.1 Overall system	14
3.2 Electric motor model	16
3.2.1 Determine the electric motor model and control parameters	17
3.3 Brake model	19
3.3.1 Heat model	19
4 CONTROL DESIGN	20
4.1 Overall control structure	20
4.2 Chassis controller	20
4.2.1 Input interpreter	21

4.3	Wheel Controller	23
4.3.1	Available torque calculation	23
4.3.2	Control Allocator	24
4.3.3	SUS controller	25
4.3.4	Brake Controller	27
5	IMPLEMENTATION OF TEST PLATFORM	29
5.1	System overview	29
5.2	Electric motors	30
5.3	Brakes	30
5.3.1	Brake discs and calipers	30
5.3.2	Pump	31
5.3.3	Pressure control	31
5.4	Electric power and wiring	33
5.5	Network, sensors and data logging	33
5.6	Controller Implementation	35
5.6.1	Implementation method	35
5.6.2	Implementation in vehicle	35
5.6.3	Data analysis and measurements	35
6	RESULTS AND VALIDATION	36
6.1	Electric motor validation	36
6.1.1	SUS torque as a function of speed	36
6.1.2	Electric power consumption for SUS and all other consumers	37
6.1.3	SUS speed controller	39
6.1.4	Complete SUS model verification	40
6.2	Brake validation	41
6.3	Control validation	42
6.3.1	Brake blending	42
6.3.2	Controller behavior	44
7	DISCUSSION	46
7.1	Components	46
7.2	Testing and validation	46
8	FURTHER WORK	48
9	REFERENCES	49
10	APPENDIX 1: SUS MODELS	50
10.1	Full SUS model	50
10.2	Simple SUS model	53

11	APPENDIX 2: MODEL USED FOR VERIFICATION OF SUS SPEED CONTROL PARAMETERS	55
12	APPENDIX 3: ELECTRIC POWER SUPPLY SCHEMATIC FOR THE TEST PLATFORM	56
13	APPENDIX 4: COMMUNICATION AND SIGNAL OVERVIEW FOR THE TEST PLATFORM	57
14	APPENDIX 5: TEST PLAN AND VERIFICATION OF SUS	58

Preface

In this thesis a test platform for testing of different concepts for a hybrid wheel loader has been developed and built. Also a brake blending system has been developed and tested on the test platform. The thesis has been carried out from September 2011 to May 2012 at CPAC Systems AB by the students Per Björe Dahl and Rickard Nilsson from Chalmers University of Technology.

Supervisor for the project has been Andy Wikjö at CPAC Systems. Examiners are Bo Egardt at the Department of Signals and Systems, Division of Automatic control, Automation & Mechatronics and Stefan Lundberg at the Department of Energy and Environment, Division of Electric Power Engineering.

The authors would like to thank Andy Wikjö, Bo Egardt and Stefan Lundberg and all the engineers on CPAC Systems for their help and guidance throughout the project. The thesis is a master thesis within the masters programs Electric Power Engineering and Systems, Control and Mechatronics.

Göteborg, May 2012

Per Björe Dahl

Rickard Nilsson

Notations

Roman upper case letters

A	Area
B	Dampening factor
F	Force [N]
F_w	Brake force [N]
I	Inertia [$\text{kg}\cdot\text{m}^2$]
K_a	Adaptive gain
K_i	Controller integral gain
K_p	Controller proportional gain
K_r	Adaptive gain
L_s	Stator inductance [H]
N_s	Rotational speed [rpm]
P	Power [W]
R_a	Active damping
R_{eff}	Effective radius on brake pad [m]
R_i	Brake disc inner radius [m]
R_o	Brake disc outer radius [m]
R_s	Stator resistance [R]
T	Torque [Nm]
V_s	Stator supply voltage [V]

Roman lower case letters

a	Acceleration [m/s^2]
f	Frequency [Hz]
i_s	Stator current [A]
i_x	Current phase x [A]
m	Mass [kg]
n_p	Number of poles
p_{brake}	Brake pressure [bar]
r_{wheel}	Brake pressure [bar]
v_x	Voltage phase x [V]

Greek lower case letters

α_c	Controller bandwidth [Hz]
γ	Tuning coefficient for adaptive gain
η	Efficiency
θ	Angle [rad]
$\dot{\theta}$	Angular velocity [rad/s]
$\ddot{\theta}$	Angular acceleration [rad/s ²]
θ_1	Estimated flux angle [rad]
μ	Friction coefficient
ψ_R	Rotor flux linkage [Wb]
ω	Rotational speed [rad/s]
ω_m	Mechanical rotational speed [rad/s]
ω_r	Electrical rotational speed [rad/s]

Abbreviations

ECU	Electronic Control Unit
ESP-block	Hydraulic pump and valve block for brake pressure control
ICE	Internal combustion engine
PMSM	Permanent magnet synchronous machine
SUS	Name of the electric motors used in the project

1 Introduction

1.1 Background

For construction equipment in general fuel efficiency is one of the most critical product attributes. Pure fuel economy improvements from the internal combustion engines are extremely expensive to develop. This creates an incitement for developing of hybrid technology.

Hybrid technology is all about energy recycling. In a conventional wheel loader all kinetic energy and energy of position are wasted through conversion into heat e.g. during braking and lowering the bucket. Instead of wasting this fairly large amount of energy the aim is to convert it to electricity and store the energy in a battery bank and later reuse it for propulsion, lifting, etc.

1.2 Problem definition

The development of a hybrid construction vehicle and in this case a hybrid wheel loader is challenging in many different areas, both on component and on system level. Examples of challenges on system level are regeneration strategies, brake blending, power management strategies and vehicle dynamics control.

For initial testing of control strategies and concepts it is faster, easier and cheaper to test on a vehicle that has the same fundamental structure as a hybrid wheel loader but much smaller.

To design a test platform for a hybrid wheel loader there are a number of problems such as

- The test platform should have nearly the same properties as the real platform
- It should be configurable and expandable
- The cost should be reasonable
- To find components with similar properties as the main components but smaller

On system level this project will focus on brake blending, i.e. the combination of electrical and mechanical braking in a hybrid vehicle. The main problems with brake blending are to make it seamless, i.e. the driver should not feel the difference between electrical and mechanical braking, and at the same time optimize the power regeneration.

1.3 Objectives

There are two main objectives with this master thesis. The first one is to develop and build a test platform that replicates a hybrid wheel-loader in a smaller scale. The test platform should represent the real application well enough to do proof of concept studies for functional development. The minimum requirements are one electric motor per wheel and a hydraulic brake by wire system i.e. the brake system should be able to be fully computer controlled. The brake by wire system should ideally be able to

brake each wheel individually. To facilitate further development the control system should be modular.

The second objective is to implement the brake blending on the test platform. When braking the maximum amount of energy shall be regenerated and for the driver the brake blending shall be fully transparent. It should not be possible to distinguish the difference between pure regenerative braking and combined regenerative and mechanical braking.

1.4 Method

The test platform will be built on an articulated chassis from a rideable lawn mower. The basic geometry correlates well with a wheel-loader chassis and is manageable in terms of size while still drivable. For practical reasons it will only be powered by batteries. At the thesis start the motors and drive chains had been fitted to the chassis. Thus it is needed to dimension, find and fit a hydraulic brake system to the chassis.

The vehicle's electric components will primarily be CPAC components used in other commercial applications, with custom software and if needed hardware. The components will be communicating with each other using the CAN protocol. The method "Model based development" will be used for developing the main control algorithm. The modeling will be done in MATLAB/Simulink and the resulting control algorithm will be implemented in the test platform through C-code generation with the automatic code generation tool TargetLink from dSPACE. The code will run on a dedicated floating point processor which gives a freedom in controller and model design in regards to computing power.

1.5 Limitations

The vehicle energy management system and the complete vehicle dynamics model is not a part of the thesis scope. The modeling and verification will only be done on the test platform and not on the full-scale hybrid wheel loader.

2 System overview

In this chapter there will be an introduction to hybrids and especially to the hybrid wheel loader concept. Basic theory for the electric motors and the brakes are presented together with a brief controller structure.

2.1 Overall system

There are several ways of designing a hybrid vehicle; most configurations can be divided into the two groups serial and parallel hybrids.

2.1.1 Parallel hybrids

In parallel hybrid systems the electric motor and internal combustion engine (ICE) are both connected to the transmission of the vehicle. It can allow for running either the electric motor or the ICE independent or combined. One advantage of parallel hybrids is that it is possible to reuse know-how and components of conventional ICE powered vehicles. The electric part of the drivetrain can be incorporated between the ICE and gearbox making it possible to use already available drivetrain technology. Another advantage is that when the ICE powers the car directly the transmission losses are low because modern gearboxes are generally very efficient (Schouten, Salman, Kheir, 2002).

2.1.2 Serial Hybrids

Serial hybrids are constructed in a different manner where the drivetrain components are entirely electric and the power to the electric motors is supplied either by batteries or by a generator connected to an ICE. In a series hybrid configuration the ICE together with the generator is only a source of electric power. In practice it means that it offers a greater flexibility in terms of power sources due to the separation between energy source and tractive force generation. However due to the additional energy conversion taking place when the ICE is powering the vehicle, there are more transmission losses which lowers the efficiency.

There are also combinations of serial and parallel hybrids; these will not be further investigated in the thesis however. In this thesis the focus will be on the serial hybrid concept.

2.1.3 Wheel loader hybrid concept

The concept for the wheel loader in this project is to have a serial hybrid with individual electric motors for each wheel and a complementary mechanical braking system. A schematic of the system can be seen in Figure 1.

The electric energy will be generated with a diesel ICE connected to a generator and between the generator and the electric motors there will be an energy storage. The energy source could also be replaced with a plug-in wall charger or fuel cell as this does not on a concept level inflict the performance of the vehicle. Range, recharging time and vehicle weight is what differs between different energy sources.

The wheel loader is equipped with mechanical brakes for two reasons. The first reason is that the electric motors in most cases are not powerful enough to produce braking torque to stop the vehicle quickly in an emergency situation. The second reason is that there must be a possibility to brake when the energy storage is full. The combination of electric and mechanical friction braking is called brake blending.

To be able to incorporate brake blending into the system the brakes must be able to be controlled electronically, “Brake by wire”. If conventional brakes should be used a source of hydraulic power is needed. Most likely it is a pump with a set of regulating valves.

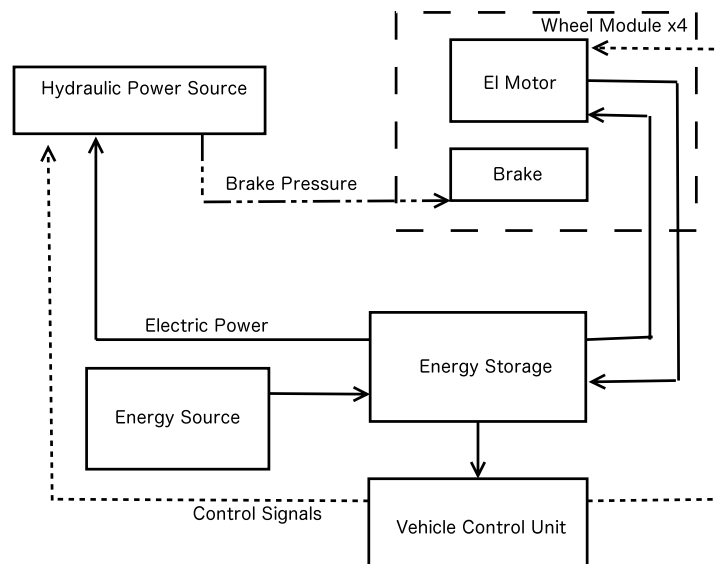


Figure 1: Flow chart of signals and energy for the serial hybrid wheel-loader system.

In the application of the wheel-loader the concept of having each wheel independently controlled is especially interesting due to the chassis layout with an articulate joint. It gives completely new possibilities in terms of steering control by helping the steering with torque vectoring which can be seen in Figure 2. It also opens up for advancements in helping the traction of the vehicle as the negative effects of having an either open or fully locked differential are avoided, as the wheels are fully independent of each other.

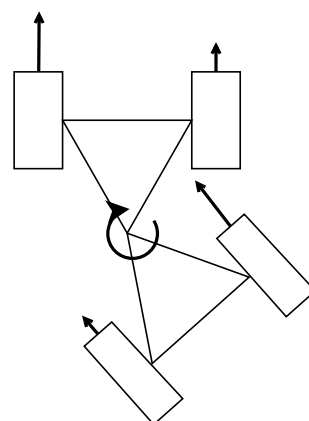


Figure 2: Torque vectoring on an articulated chassis, a longer arrow indicates a higher tractive force. The chassis constraints lead to a rotating action around the articulate joint which changes the steering angle.

2.2 Electric motors

The test platform in the project is equipped with electric motors of permanent magnet synchronous machine type (PMSM). The benefit of using synchronous machines is that the speed is well defined as they run synchronously. For PMSM machines also the efficiency is high compared to induction machines because no magnetising current is needed. The disadvantage with PMSM is that they are expensive due to high cost of the magnets and construction difficulties (Harnefors, 2002).

2.2.1 Construction

A PMSM can be seen as an inside out DC machine with the windings in the stator instead of in the rotor. The magnetic field is generated by permanent magnets that are assembled on the rotor (surface mounted) or inside the rotor (buried). Rotors with surface mounted magnets are easier to manufacture but are mechanically weak at high speeds. The other way around yields for rotors with buried magnets (Harnefors, 2002).

PMSM are always running at a speed determined by the frequency of the supply voltage. The only way to obtain different speeds on a PMSM when connected to a fixed frequency is to use machines with different number of poles. The speed is given by *Equation 1* where N_s is the speed in rpm, f is the supply frequency in Hz and n_p is the number of poles.

$$N_s = \frac{60f}{n_p} \quad \text{Equation 1}$$

If the load torque is changing, the rotor speed is not changing as can be seen in Figure 3 but the load angle is changing. The load angle is the angle between the stator magnetic field and the rotor magnetic field. At no load the load angle is ideally 0 degrees and the maximum torque is reached when the load angle is 90 degrees. Above 90 degrees load angle the PMSM goes into an unstable region where it will fall out of synchronisation and stall.

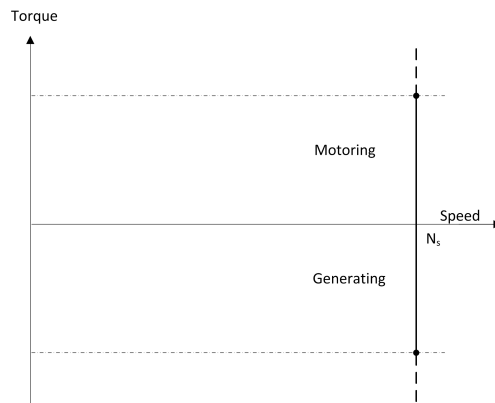


Figure 3: Speed – torque curve for a PMSM. The speed is constant for a constant supply frequency.

Because the rotor speed is related to the stator supply voltage frequency, the supply frequency has to be changed at motor start-up and speed changes. This means that the PMSM has to be powered by an inverter to be able to run at different speeds and start-up without auxiliary starting equipment. To be able to synchronise the supply frequency with the rotor speed a rotor position sensor or some algorithm to estimate the rotor position must be used (Hughes, 2006).

2.2.2 Operation

To be able to supply the PMSM with a variable frequency and voltage magnitude an inverter is needed. The inverter output can either be sinusoidal or square-wave depending on the control strategy. In this thesis only inverters with a sinusoidal output will be considered. The most common setup for a three phase inverter is to use a three leg inverter with two switches in each leg and the motor connected in a star connection which can be seen in Figure 4.

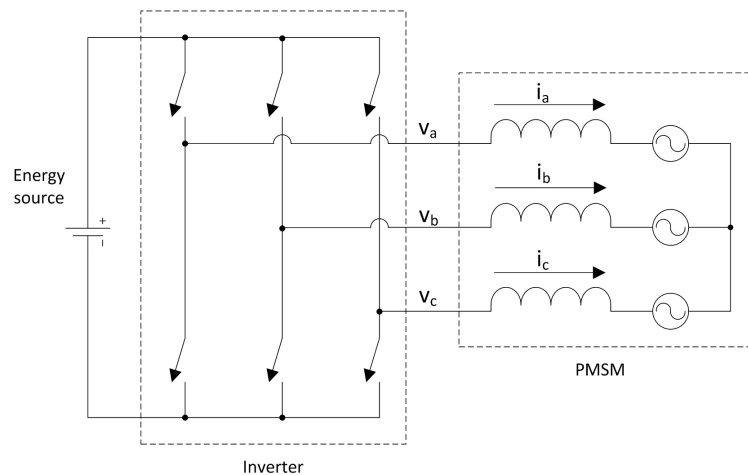


Figure 4: Three phase inverter and a star connected electrical motor.

To obtain the sinusoidal output the switches are controlled by comparing a triangular wave with three reference sinusoidal control voltages that are 120° out of phase as shown in Figure 5. If the sinusoidal control voltage is greater than the triangular wave the lower switch in the leg is opened and the upper switch is closed. When the control voltage is lower than the triangular wave the relationship is the other way around. This creates a PWM voltage between the phases of the PMSM which is shown in Figure 6. The average value of the PWM voltage over one period of the triangular wave is equal to the reference voltage. The average voltage is shown in Figure 6 as a dashed line. Because the PMSM windings acts like an inductive filter the current in the PMSM becomes sinusoidal (Mohan, Undeland, Rohan, 2003).

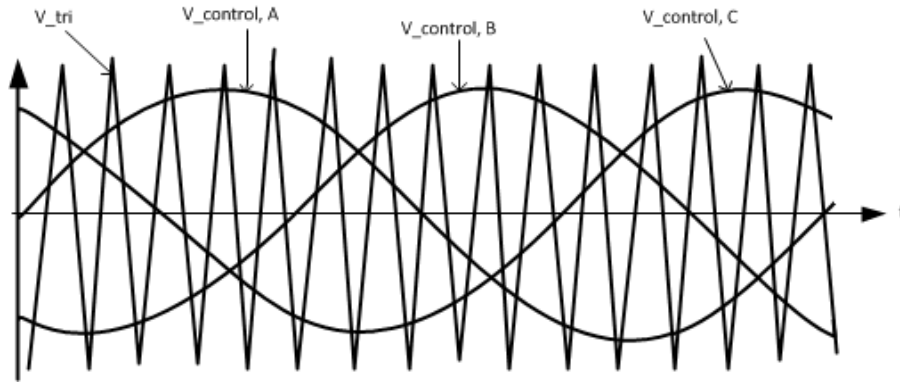


Figure 5: Triangular wave compared with three sinusoidal control waves for control of the switches in the converter (Mohan, Undeland, Rohan, 2003).

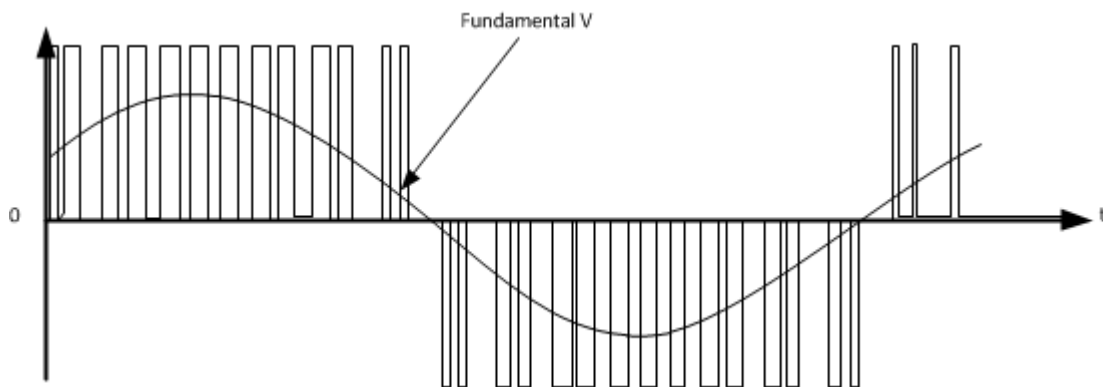


Figure 6: Output voltage between two phases in the converter (Mohan, Undeland, Rohan, 2003).

2.2.3 Mathematical model and dq representation

The equivalent circuit for the stator winding in the PMSM can be modelled as a resistance, an inductance and a back-emf for a non-salient PMSM and the equivalent circuit is shown in Figure 7.

The three stator equations for the equivalent circuit in Figure 7 are given by *Equation 2*, *Equation 3* and *Equation 4* where v_x is the phase x supply voltage, i_x the phase x stator current, R_s the stator winding resistance, L_s the stator winding inductance, ω_r the electrical speed of the rotor, ψ_R the flux linkage from the magnets and θ the rotor angle.

$$v_a = R_s i_a + L_s \frac{di_a}{dt} - \omega_r \psi_R \sin(\theta) \quad \text{Equation 2}$$

$$v_b = R_s i_b + L_s \frac{di_b}{dt} - \omega_r \psi_R \sin\left(\theta - \frac{2}{3}\pi\right) \quad \text{Equation 3}$$

$$v_c = R_s i_c + L_s \frac{di_c}{dt} - \omega_r \psi_R \sin\left(\theta - \frac{4}{3}\pi\right) \quad \text{Equation 4}$$

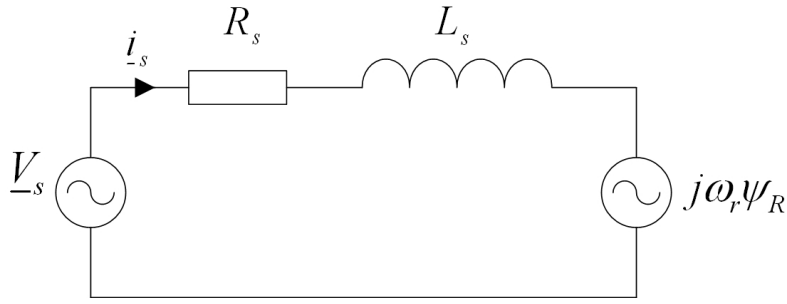


Figure 7: The equivalent circuit for a non salient PMSM

The active power that creates the mechanical output power of the PMSM is consumed in the rotor back-emf shown as a voltage source in the equivalent circuit in Figure 7. In a three phase PMSM with the voltage and current expressed in peak values the mechanical output power from the PMSM is given by Equation 5 and the torque produced is given by Equation 6. In the equations ω_m represents the mechanical output speed (Harnefors, 2002).

$$P_e = \frac{3}{2} \operatorname{Re}\{j\omega_r\psi_R i_s\} = \frac{3\omega_r}{2} \operatorname{Im}\{\psi_R i_s\} \quad \text{Equation 5}$$

$$T_e = \frac{P_e}{\omega_m} = \frac{P_e n_p}{\omega_r} = \frac{3n_p}{2} \operatorname{Im}\{\psi_R i_s\} \quad \text{Equation 6}$$

The PMSM needs a sinusoidal input current to run but from a control system perspective it is easier to control a DC-quantity. For electric motors this is solved by transforming the three phase (abc reference) sinusoidal currents to the dq reference frame where the voltages become DC at steady state. The main idea in the transformation is to let the dq-coordinate system rotate with the rotor and the flux generated by the rotor. This transformation is done in two steps. First it is assumed that the sum of the currents in to the PMSM is zero at all times. This is valid if the PMSM is star connected and no neutral connector is used as shown in Figure 8.

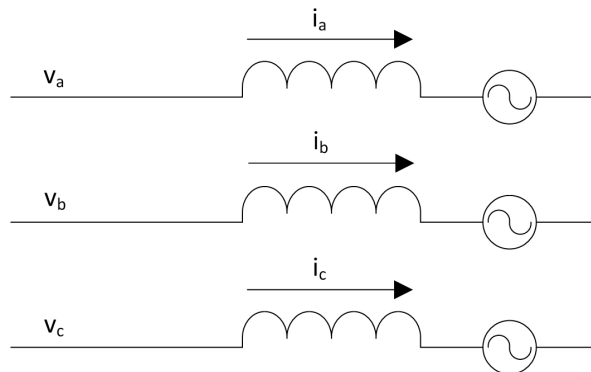


Figure 8: Electric motor star connected

When the sum of the currents equals zero the abc system can be transformed to a system with only two variables (alfa-beta system). The transformation is given by *Equation 7* and on complex form the alfa-beta voltage can be represented by *Equation 8*.

$$\begin{bmatrix} v_\alpha \\ v_\beta \end{bmatrix} = \begin{bmatrix} \frac{2}{3} & -\frac{1}{3} & -\frac{1}{3} \\ 0 & \frac{1}{\sqrt{3}} & \frac{1}{\sqrt{3}} \end{bmatrix} \begin{bmatrix} v_a \\ v_b \\ v_c \end{bmatrix} \quad \text{Equation 7}$$

$$\underline{v}_s^{\alpha\beta} = v_{s,\alpha} + jv_{s,\beta} \quad \text{Equation 8}$$

The alfa-beta voltages and currents are also sinusoidal and to get the variables to a DC value a transformation to dq coordinates has to been done. The transformation to and from the dq reference frame is done respectively with *Equation 9* and *Equation 10* where θ_1 is the estimated flux angle.

$$\underline{v}^{dq} = e^{-j\theta_1} \underline{v}^{\alpha\beta} \quad \text{Equation 9}$$

$$\underline{v}^{\alpha\beta} = e^{j\theta_1} \underline{v}^{dq} \quad \text{Equation 10}$$

When transforming the three stator equations for the PMSM (*Equation 2 - Equation 4*) using the dq method the result is given by *Equation 11* if the field orientation is perfect, i.e. $\theta_1 = \theta$.

$$\underline{v}_s^{dq} = R_s \underline{i}_s^{dq} + L_s \frac{d\underline{i}_s^{dq}}{dt} + j\omega_r \psi_R + j\omega_r L_s \underline{i}_s^{dq} \quad \text{Equation 11}$$

With *Equation 11* divided into the real part (d) and the imaginary part (q) the stator equation is given by *Equation 12* and *Equation 13*.

$$v_{s,d} = R_s i_{s,d} + L_s \frac{di_{s,d}}{dt} - \omega_r L_s i_{s,q} \quad \text{Equation 12}$$

$$v_{s,q} = R_s i_{s,q} + L_s \frac{di_{s,q}}{dt} + \omega_r \psi_R + \omega_r L_s i_{s,d} \quad \text{Equation 13}$$

With perfect field orientation the torque equation is given by *Equation 14*.

$$T_e = \frac{3n_p}{2} \psi_R i_{s,q} \quad \text{Equation 14}$$

2.2.4 Control of PMSM

One specific thing to keep in mind when designing controllers for electric motors is that the electrical characteristics in the motor are much faster than the characteristics of the mechanical load. One proposed control strategy which is shown in Figure 9 is therefore to use two controllers, one fast inner controller that controls the electrical system (control of the current) and a slower outer controller that controls the mechanical system (control of the speed) (Mohan, Undeland, Rohan, 2003).

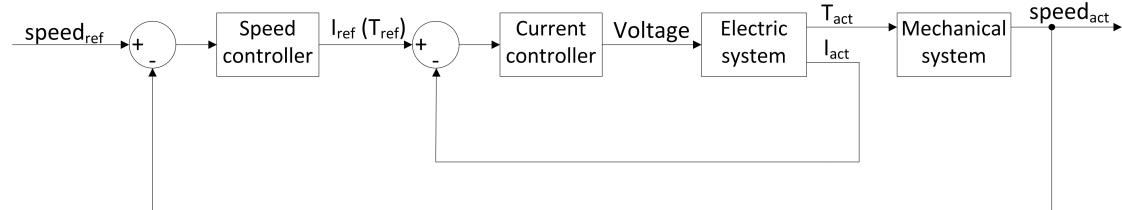


Figure 9: Proposed control structure for electric motor.

The electrical system is modeled from the PMSM stator *Equation 11*. For the control of the PMSM the dq-transformed values will be used because these are DC values in steady state. When transformed to Laplace the stator equation in dq-coordinates will be given by *Equation 15* and modeled as in Figure 10.

$$\underline{v}_s^{dq} - j\omega_r \psi_R = \underline{i}_s^{dq} (R_s + sL_s + j\omega_r L_s) \quad \text{Equation 15}$$

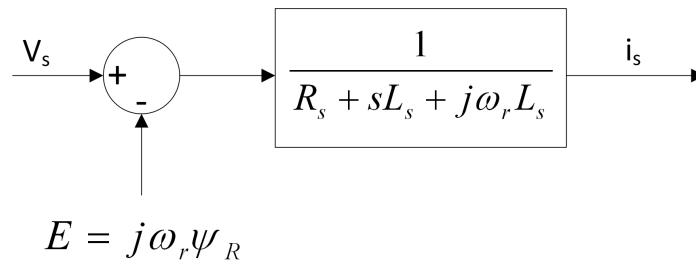


Figure 10: PMSM electric motor model based on Equation 15.

To obtain an efficient control of the electric motor, compensation can be done for the “disturbances” in the electric motor transfer function. The back-emf ($E=j\omega_r\psi_R$) and the cross-coupling ($j\omega_r L_s$) can be seen as disturbances and can be compensated for by estimations of the back-emf and the cross-coupling. To make these estimations accurate there is a need for a good measurement of the speed. In the model in

Figure 11 it can be seen how the compensation is done and where $\hat{\psi}_R$, $\hat{\omega}_r$ and \hat{L}_s are estimations of respective variable. Modeling of the electric motors and controller design is presented in chapter 3.2.

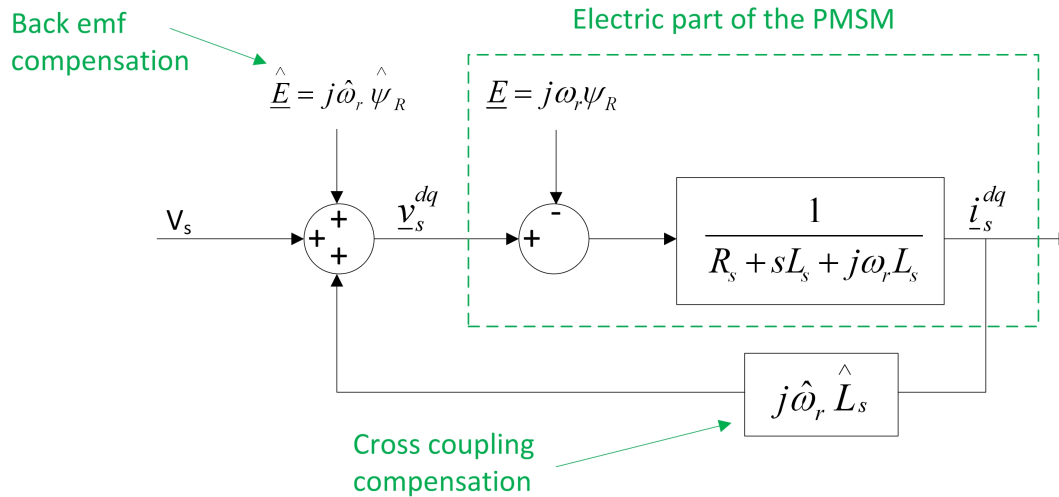


Figure 11: Electric motor model with compensation of back-emf and cross-coupling.

2.3 Brake system

Brakes general working principle is converting mechanical energy into heat. In heavy machinery and road vehicles there are mainly two types of brakes used, drum brakes and disc brakes. The scope of this project has been looking into the dynamics of the disc brake.

2.3.1 Heat dependent dynamics

Crucial to the disc brake dynamics is its temperature dependency. As the heat builds up in the brake disc, the friction coefficient between the disc and the friction material changes (Ostermeyer, Müller, 2005). The friction coefficient varies with a factor of over 40% (Madås D, Lai H, 2011), thus it is essential to take the brake temperature into account to estimate the brake torque generated by a certain brake pressure.

It is relatively easy to calculate the energy absorbed into the brake disc, since it is given by the brake power (brake torque x speed), under the assumption that all power generated is transformed into heat in the brake disc. This is a simplification of the real case as the brake pads and brake caliper will absorb some heat as well. However 95% of the heat will go into the brake disc (Mägi, Melkersson 2008). What is very difficult to model is the amount of energy dissipated by the disc brake.

There are in principle two major types of disc brakes, ventilated and solid brakes as shown in Figure 12. It is not a feasible task to calculate the heat dissipation of ventilated brakes analytically, Finite Element methods are required (Voller, Tirovic, Morris, Gibbens 2003). In the case of the solid disc it is easier making analytical estimations of the heat transfer. An analytical model tuned with measured data could provide data usable enough for estimating a temperature with accuracy enough to predict big changes in friction coefficient.

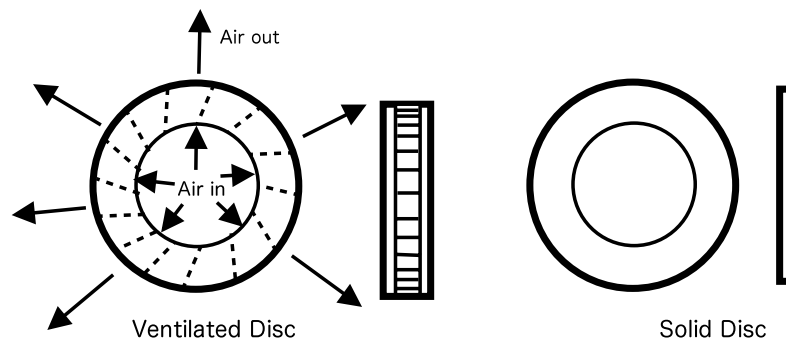


Figure 12: Ventilated vs. solid brake disc, in the ventilated brake disc air enters through ventilation channels in the centre of the disc, the grooves are designed to work as a radial fan.

There are three modes of heat transfer, conduction, convection and radiation. Conduction is heat transfer within one solid medium or two solid mediums, convection is the transfer of heat between a solid medium and a viscous medium and radiation is the energy that radiates from the surface of a medium.

Conduction heat propagation within the brake disc is significant enough to take into account for ventilated brake discs as the heat needs to transfer from the outer surface to the inner ventilation duct. Solid brake discs have the same heat uptake zone as main heat dissipation zone which makes the conduction mode less significant.

In the convection case the heat is transferred to the surrounding air and the airflow of the dissipation surface is the biggest variable. Thus it is dependent on the speed difference between the brake disc surface and the surrounding air.

The radiated heat transfer is mainly dominant for high temperatures as opposed to convection which is the dominant heat transfer mode at lower temperatures (Incropera, DeWitt, Bergman, Lavine 2007).

It is a very complex task to accurately model the disc brake temperature and also computationally demanding. Thus in this master thesis a small model involving radiation and speed-dependent convection has been implemented in MathWorks Simscape.

2.3.2 Limits, transients in applying brakes

Generally the limit in braking force is set by the mechanical grip of the tires and not the amount of force the brakes can generate. This assumes a well dimensioned system. When applying the brakes a transient force can occur the moment the friction material hits the disc. What is needed to determine through physical testing is if the transient is big enough to consider in the control application. The most probable case is that the transient is too fast to be accurately measure and compensate for. Thus it can be expected that the transient will be damped out due to wheel, brake and chassis flex. The same will occur when releasing the brake pressure; a small dragging force can be expected. Initially a small drag before the floating disc “bumps” the brake pads into a non dragging position.

2.3.3 Regenerative brake controller

As previously mentioned electric motors are in most vehicle applications not powerful enough to stop the vehicle in an emergency braking situation and therefore it is also needed to equip the vehicle with conventional mechanical brakes.

For regenerative braking there are two main strategies to control the brakes, in series or in parallel. Series control of the brakes means that first are the electrical brakes utilized to its maximum and after that the mechanical brakes are used. Parallel control of the brakes means that the mechanical and electrical brakes are used together during the whole braking procedure. The advantage with series regenerative braking is that the regenerated energy can be maximized and the advantage with parallel regenerative braking is that control of the system is simpler to implement (Shuang, Junzhi, Lifang, 2009).

The main difficulty in a serial braking strategy is to ensure a smooth and seamless transition from regenerative braking to a combined braking effort. It requires a deep understanding on the dynamics of the components to ensure a linear braking response as a sudden change in braking effort could lead to hazardous situations.

2.4 Controller

There are multitudes of ways of implementing a vehicle controller. Due to the complexity of the project given the limited time frame the most advanced types of control algorithms have not been considered.

The vehicle controller is a network of basic controllers forming a complex system. This system can be seen as different layers of control; in the scope of this project the whole chain from low-level control to high-level control is covered. The low-level control is on a device level, for example delivering a fast and precise brake pressure. The high level control is on a vehicle level regulating the vehicle motion, sending request to midlevel or low level controller.

A modular structure makes the controller scalable, enabling adding additional or replacing input and output devices. Separating high level features from motors and brakes makes it possible to add and remove features on the vehicle.

The controller structure is more thoroughly reviewed in the implementation part of the thesis.

3 Implementation of models

The purpose for modeling the parts in the wheel loader was to be able to design good controllers by doing simulations and by that decrease the testing time. In this chapter models for the overall wheel loader, the electric motors and the brakes will be presented.

3.1 Overall system

The overall system model was based around a simple model of the chassis to create an envelope for the more advanced motor, brake and control models. The focus was on longitudinal acceleration, which in its simplest form is $F=ma$. Generally when doing a vehicle model, tire slip has to be implemented in some way. By restricting the model use for primarily longitudinal acceleration decent accuracy can be achieved without implementing a slip model:

$$F = ma \quad \text{Equation 16}$$

$$F = (T_{FL} + T_{FR} + T_{RR} + T_{RL})r_{wheel} \quad \text{Equation 17}$$

$$T_{wheel} = \eta(N * T_{motor}) + T_{brakes} \quad \text{Equation 18}$$

where T_{FL} is the torque from the front left wheel, T_{FR} is the torque from the front right wheel, T_{RR} is the torque from the rear right wheel, T_{RL} is the torque from the rear left wheel, r_{wheel} is the wheel radius, T_{wheel} the resulting torque acting on one wheel, T_{motor} the torque from the electric motors, T_{brakes} the torque generated by the brakes, N is the gear ratio and η is the efficiency in the chain drive.

In terms of simulating longitudinal acceleration these simple equations go a long way. However due to the geometry of an articulated vehicle where the wheel torque has a big impact on steering angle, i.e. torque vectoring; also a geometrical model of the chassis had to be implemented. Instead of implementing a tire slip model, tire slip was simulated by adding a large dampening factor to the chassis inertia.

The chassis model is built upon rigid body dynamics, and is divided into two coordinate systems which can be seen in Figure 13. The first coordinate system is anchored in the centre of mass of the rear frame and the second is on the articulate joint and is anchored in the front chassis.

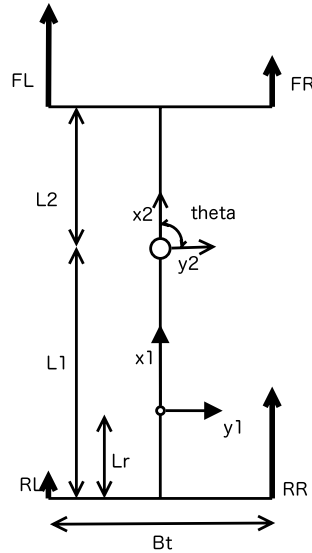


Figure 13: Chassis model with chassis dimensions ($L1$, $L2$, Lr and Bt), chassis coordinate systems ($x1$, $y1$ and $x2$, $y2$) and forces acting on the chassis (FL , FR , RL , RR)

Force vectors

$$F_{FL} = (F_{FL}, 0, 0) \quad \text{Equation 19}$$

$$F_{FR} = (F_{FR}, 0, 0) \quad \text{Equation 20}$$

$$F_{RL} = (F_{RL}, 0, 0) \quad \text{Equation 21}$$

$$F_{RR} = (F_{RR}, 0, 0) \quad \text{Equation 22}$$

Front axle coordinates expressed in coordinate system 2

$$W_{FL2} = (L2, -\frac{Bt}{2}, 0) \quad \text{Equation 23}$$

$$W_{FR2} = (L2, \frac{Bt}{2}, 0) \quad \text{Equation 24}$$

Pivot point coordinates expressed in coordinate system 1

$$Pivot_1 = (L1 - Lr, 0, 0) \quad \text{Equation 25}$$

Rear axle coordinates expressed in coordinate system 1

$$W_{RL1} = (-Lr, -\frac{Bt}{2}, 0) \quad \text{Equation 26}$$

$$W_{RR1} = (-Lr, \frac{Bt}{2}, 0) \quad \text{Equation 27}$$

Vehicle centre of mass

$$M_{v1} = (0, 0, 0) \quad \text{Equation 28}$$

Transformation from coordinates system 2 to 1

Rotational matrix

$$R_2 = \begin{pmatrix} \cos(\theta) & -\sin(\theta) & 0 \\ \sin(\theta) & \cos(\theta) & 0 \\ 0 & 0 & 0 \end{pmatrix} \quad \text{Equation 29}$$

$$W_{FL1} = R_2 W_{FL2} + Pivot_1 \quad \text{Equation 30}$$

$$W_{FR1} = R_2 W_{FR2} + Pivot_1 \quad \text{Equation 31}$$

The torque around the pivot point M_0 can be calculated with the cross products of the force vectors.

$$M_0 = (R_2 F_{FL}) \times (W_{FL1} - Pivot_1) + (R_2 F_{FR}) \times (W_{FR1} - Pivot_1) + (F_{RL}) \times (W_{RL1} - Pivot_1) + (F_{RR}) \times (W_{RR1} - Pivot_1) \quad \text{Equation 32}$$

Once the torque is calculated the angular acceleration of the articulation angle can be estimated. At this point in the calculation the model lacks details as the slip and lateral forces from the tires. Instead the inertia I and dampening factor B was tuned to a crude estimation, set very high to simulate the tire forces on the chassis. This is given by *Equation 33* where $\dot{\theta}$ is the angular velocity and $\ddot{\theta}$ is the angular acceleration.

$$\ddot{\theta} = \frac{M_0}{I} - B \dot{\theta} \quad \text{Equation 33}$$

3.2 Electric motor model

The electric machine used to build the test platform in the project is a PMSM with built in inverter and controller. The electric machine used is called SUS. The control signal sent to the SUS is a speed reference and as feedback the SUS gives the actual speed and actual torque. As most of the parameters for the SUS were unknown, the modeling work has been “reverse engineering” of the SUS from data given in specifications for the SUS.

Both a full SUS model and a simple model of the SUS have been developed. The simple model was used in the vehicle model to increase the simulation speed when simulating the behavior for the complete vehicle. The base for the model is the equations in Chapter 2.2.

When modeling the SUS it has been assumed that

- there is one current and one speed controller in the SUS
- the controllers are PI controllers and the parameters for the current controller are determined with the IMC method
- the current controller has compensation for back-emf and decoupling, anti-windup and active damping
- the speed controller has no anti-windup

To get the model to fully correspond to the SUS specification, a torque limit has been implemented. Also an available torque calculator has been implemented to give information to the overall vehicle model. When determining the SUS control parameters it was assumed that the mechanical dynamics in the system are much slower than the electrical dynamics and that the internal model control (IMC) method was used to set the controller parameters.

3.2.1 Determine the electric motor model and control parameters

Values for the parameters for the electric motor part of the SUS were found from the datasheets and by calculating values from the datasheet parameters. The winding resistance, the winding inductance and a basic speed-torque relationship was found from the data sheet.

The flux linkage was estimated with *Equation 13* as base, ideally at full speed the back emf equals the supply voltage and the current in the windings therefore goes towards zero. With the assumptions above *Equation 13* can be simplified to *Equation 34* and the flux linkage can be estimated.

$$\psi_R = \frac{v_{s,q}}{\omega_m n_p} \quad \text{Equation 34}$$

When determining the electrical control parameters it was assumed that the electrical dynamics are much faster than the mechanical dynamics. The overview of the total model with the prerequisite given earlier can be found in Figure 14.

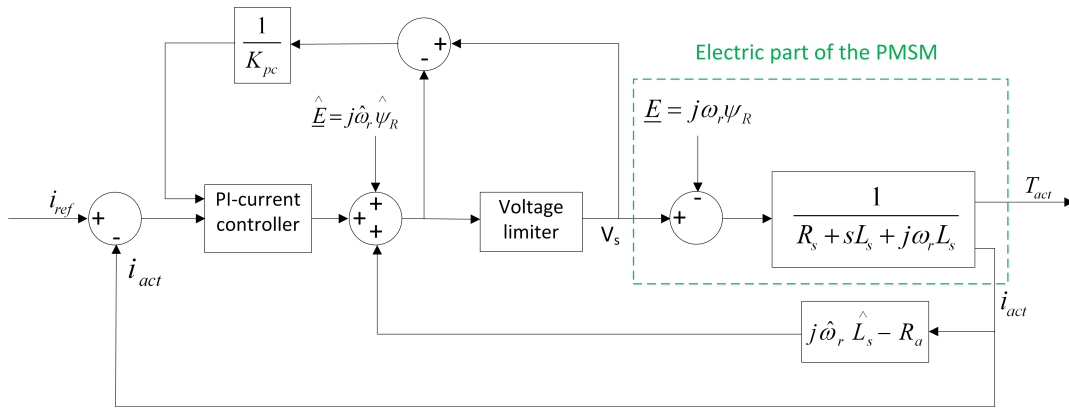


Figure 14: Current controller and electrical parts of the SUS.

If the PI-part of the controller is set to be F and the SUS together with the compensation for back-emf and cross-coupling and active damping is set to be G the transfer function for the electrical subsystem can be represented by *Equation 35*. The PI controller in F is given by *Equation 36* and the G block is given by *Equation 37* if the compensation parameters are assumed to be perfect, i.e. $\hat{\psi}_R = \psi_R$, $\hat{L}_m = L_m$ and $\hat{\omega}_r = \omega_r$.

$$\frac{i_{act}}{i_{ref}} = \frac{FG}{1 + FG} \quad \text{Equation 35}$$

$$F = K_{pc} + \frac{K_{ic}}{s} \quad \text{Equation 36}$$

$$G = \frac{1}{R_s + sL_s + R_a} \quad \text{Equation 37}$$

When determining the control parameters for the current controller with the IMC method the current controller parameters were set according to *Equation 38* where α_c is the bandwidth of the closed loop system. The active damping was set to make the system (G) have the same bandwidth as the controller. Expressions for the control parameters are presented in *Equation 39*, *Equation 40* and *Equation 41*, and in these equations estimations of the parameters are used, i.e. \hat{R}_s and \hat{L}_s .

$$\frac{\alpha_c}{s + \alpha_c} = \frac{i_{act}}{i_{ref}} = \frac{F * G}{1 + F * G} \quad \text{Equation 38}$$

$$K_{pc} = \alpha_c \hat{L}_s \quad \text{Equation 39}$$

$$K_{ic} = \alpha_c (\hat{R}_s + R_a) \quad \text{Equation 40}$$

$$R_a = \hat{L}_s \alpha_c - \hat{R}_s \quad \text{Equation 41}$$

The speed controller parameters were determined from tests on the SUSes. The result from the test is found in chapter 6.1.3 SUS speed controller.

The model of both the full and the simple SUS Simulink model can be found in Appendix 1: SUS models.

3.3 Brake model

The basic dynamics of a disc brake is easy to understand: a force applied on a brake compound interacting with a rotating disc and creating a braking torque on the disc.

To simplify the calculations an estimation of a point force can be made instead of integrating over the entire pad-area. Where this point force interacts is called the effective radius. In the case of brand new pads and disc it is necessary to calculate the effective radius of where the force is applied to get the resulting torque. The effective radius is calculated with (Mägi, Melkersson 2008):

$$R_{eff} = \frac{2(R_o^3 - R_i^3)}{3(R_o^2 - R_i^2)} \quad \text{Equation 42}$$

where R_{eff} is the effective radius, R_o is the outer radius, and R_i is the inner radius.

With worn in brake pads the case is different however, as the wear of the brake pads will be higher towards the outer radius than the inner due to higher relative speed of the brake disc surface. The result is a higher pressure towards the centre of disc and thus a migration of the effective radius towards the centre of the disc. This results in a lower generated specific torque for a certain brake pressure. A common assumption is that the wear will reach a steady state around the point where R_{eff} equals the average radius of the disc (Mägi, Melkersson 2008):

$$R_{eff} = \frac{R_o + R_i}{2} \quad \text{Equation 43}$$

The piston force F_w is a direct relation to the brake pressure p_{brake} , the piston area A_{piston} and the number of pistons $N_{pistons}$:

$$F_w = p_{brake} A_{piston} N_{pistons} \quad \text{Equation 44}$$

The braking torque T_w generated from the brake force depends on the friction coefficient μ and the effective radius:

$$T_w = \mu F_w R_{eff} \quad \text{Equation 45}$$

3.3.1 Heat model

A heat model of the brakes was made and implemented in Simscape, which is a module in Simulink; it was however deemed redundant as the temperature rise was negligible in the short braking cycles with the test platform. Thus it is not included in the scope of this thesis.

4 Control design

4.1 Overall control structure

The controller structure shown in Figure 15 is divided into two main logic parts, the chassis controller and the wheel controllers. The chassis controller translates driver inputs to a requested torque for each wheel. It also handles limits like maximum speed and steering angle etc. The chassis controller does not determine which actuator that should carry out the request.

The wheel controllers are for the chassis controller just actuators, basic operation is that it takes a torque request and translates it to a reference signal to the electric motors and a reference brake pressure. The regenerative braking strategy rule set is thus implemented in the wheel controllers and is transparent to the chassis controller.

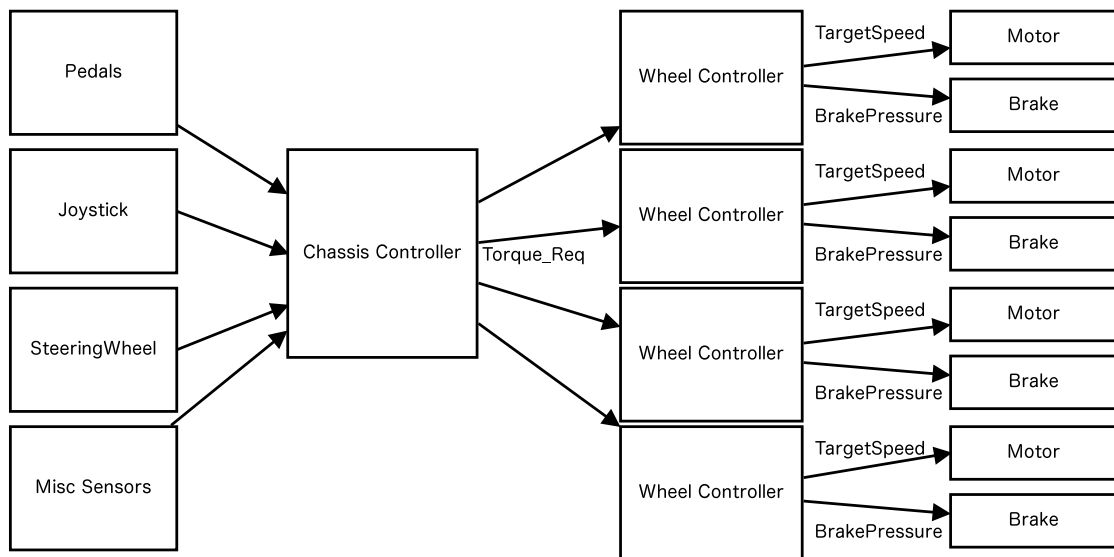


Figure 15: Overall control structure for test platform.

4.2 Chassis controller

The chassis controller shown in Figure 16 consists of a few logic blocks, where the input interpreter block has been the main focus. The steer angle controller is a simple PI loop and has not been the focus of the master thesis, it is there as merely a place holder for a future more advanced “Steer by wire” algorithm. Likewise is the vehicle speed estimator implemented as simple as possible. It is an average speed of all four wheels not taking wheel slip into account.

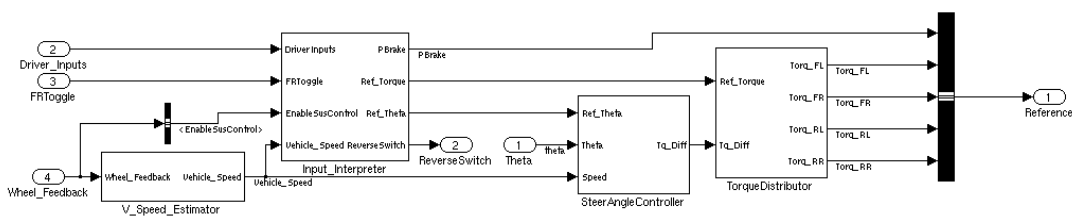


Figure 16: Chassis controller on test platform.

4.2.1 Input interpreter

The input interpreter is a set of rules that based on the input variables sends out a reference torque for the vehicle. The input interpreter shown in Figure 17 has been implemented in Stateflow for good visualization and compatibility with the TargetLink C-code generator used. Stateflow is a Matlab/Simulink component for creating efficient state machines.

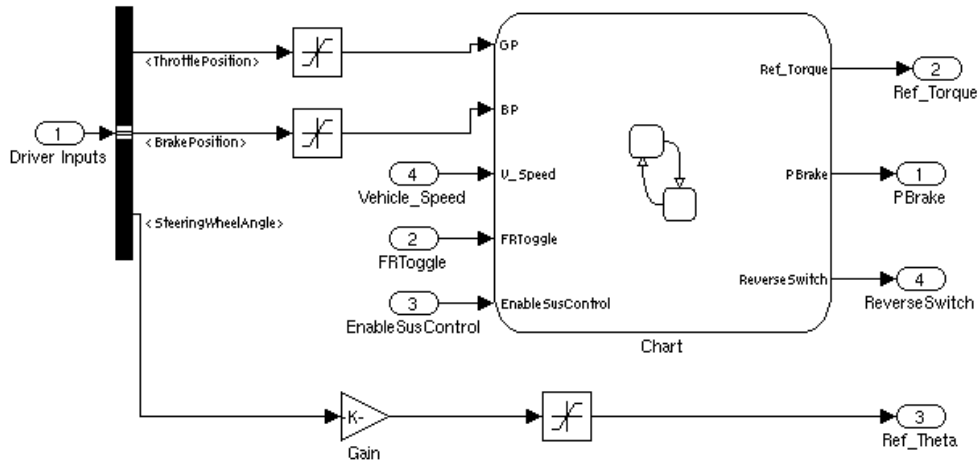


Figure 17: Input interpreter in the chassis controller for the test platform.

The state flow chart which is shown in Figure 18 makes up a state machine that depending on what mode the vehicle is operating in translates pedal movements to torque requests. Transitions between the states are set up with rules and conditions. The input interpreter does not handle steering control, it simply sets up a reference torque for the whole vehicle forwards and backwards. It does allow for easy extension for either implementing more advanced states or additional functions.

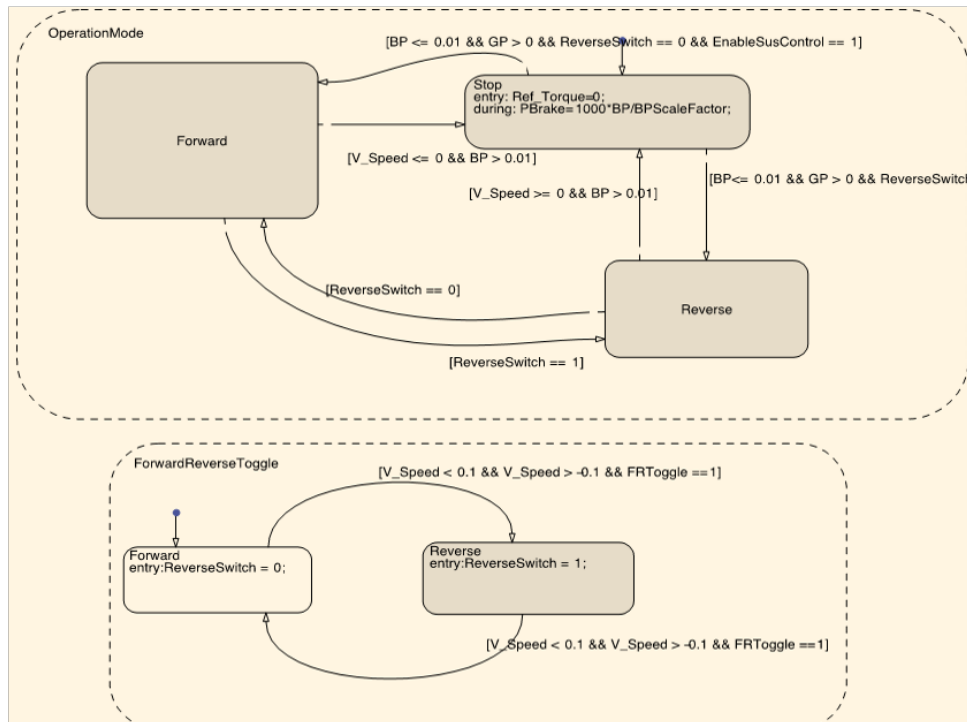


Figure 18: State flow control of the torque requests in the chassis controller for the test platform.

The stateflow consists of two parallel state machines, the ForwardReverseToggle and OperationMode state machines. The ForwardReverseToggle handles the “gear” change behaviour and it does not allow the operator to change gear until the vehicle speed is almost stopped ($<0,1\text{m/s}$). The OperationMode state machine implements different pedal behaviour depending on gear and vehicle speed. BP is brake pedal value and GP is the gas pedal value, both with a scale from 0 to 1 for the whole stroke. In the forward and reverse states, the scaling from pedal positions to requested wheel torque is done. A crude speed limiter is also implemented limiting the speed of the vehicle. In Figure 19 the forward state is shown in detail.

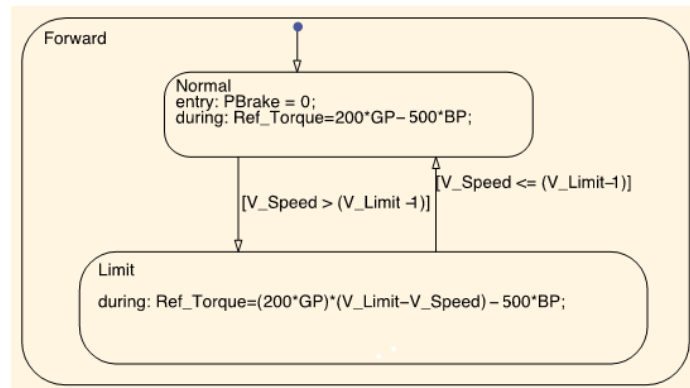


Figure 19: The pedal movement to wheel torque request scaling are done in the forward and reverse sub-states.

4.3 Wheel Controller

The wheel controller which is shown in Figure 20 consists of three different subsystems and a state machine. The state machine contains a rule set that determines which actuator (electrical motor or mechanical brakes) to use and how to calculate the torque split between electric and mechanical brakes. The subsystems handle brake and motor control and motor modelling. The subsystems and state machine will be further described in the following subchapters.

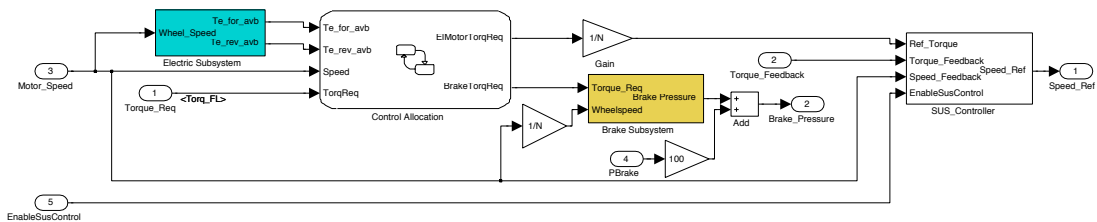


Figure 20: Wheel controller for the test platform.

4.3.1 Available torque calculation

The available torque calculation which is shown in Figure 21 is derived from the more advanced motor models used in the vehicle model. It is translated into a lookup table based on the speed input and some simple logic to determine direction of travel. Estimating how much torque that is available serves two purposes. The foremost usage is for calculating the brake blending torque split i.e. how much braking torque the motor can generate. But it is also used for anti-windup of the motor controller, making sure that the torque request does not exceed the maximum motive torque available at any given time.

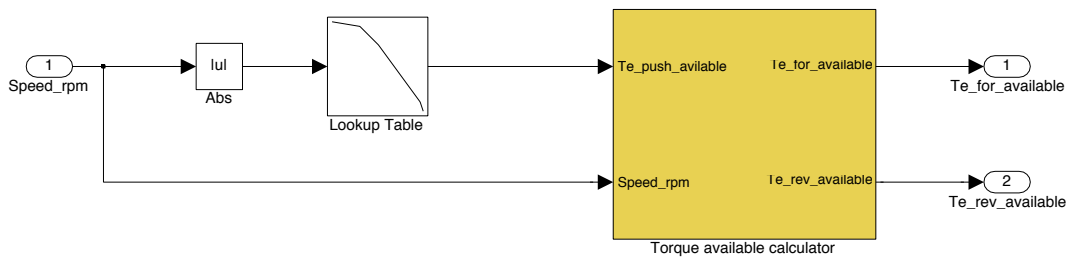


Figure 21: Available torque calculator in the wheel controller for the test platform.

4.3.2 Control Allocator

It is called a control allocator but is in reality a state machine with rules on torque split based on torque request, direction of motion and available torque estimation from the motors. The stateflow diagram in Figure 22 with states and transitions is a realisation of the relatively simple rule set given by *Equation 46* and *Equation 47*. Where T_{el} is electric torque, T_{brake} is braking torque, T_{req} is requested torque, T_{regen} is available regenerative torque and T_{drive} is drive torque.

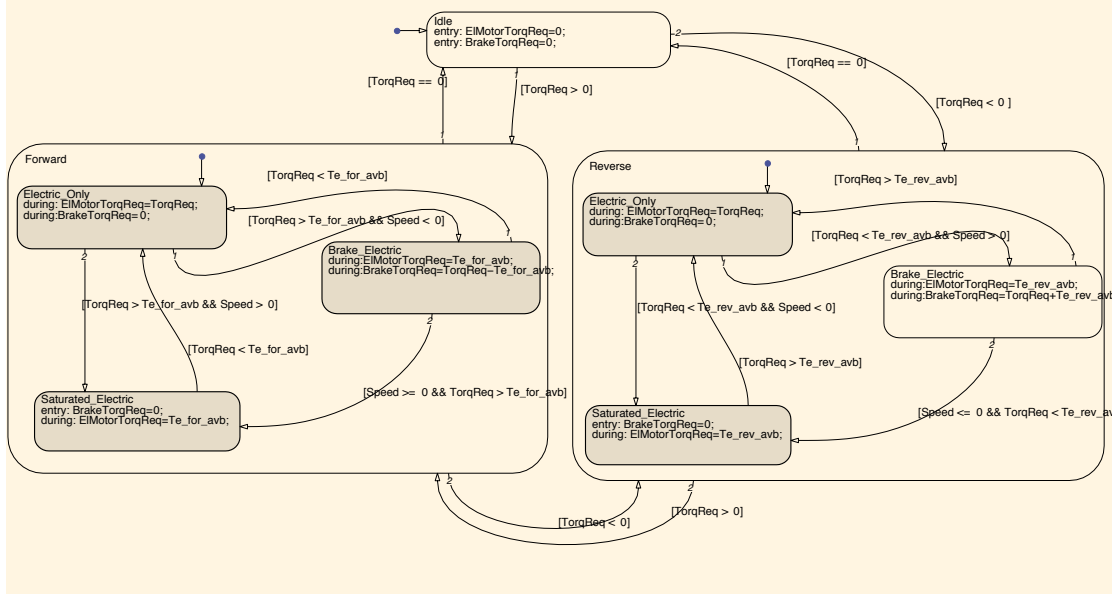


Figure 22: Control allocator in the wheel controller for the test platform.

$$T_{el} = \begin{cases} T_{req}, & T_{regen} < T_{req} < T_{drive} \quad \forall \omega \geq 0 \\ T_{drive}, & T_{req} \geq T_{drive} \quad \forall \omega \geq 0 \\ T_{regen}, & T_{req} \leq T_{regen} \quad \forall \omega \geq 0 \\ T_{req}, & T_{drive} \leq T_{req} < T_{regen} \quad \forall \omega < 0 \\ T_{drive}, & T_{req} \leq T_{drive} \quad \forall \omega < 0 \\ T_{regen}, & T_{req} \geq T_{regen} \quad \forall \omega < 0 \end{cases} \quad \text{Equation 46}$$

$$T_{brake} = \begin{cases} 0, & T_{req} \geq T_{regen} \quad \forall \omega \geq 0 \\ T_{req} - T_{regen}, & T_{req} < T_{regen} \quad \forall \omega \geq 0 \\ 0, & T_{req} \leq T_{regen} \quad \forall \omega < 0 \\ T_{req} + T_{regen}, & T_{req} > T_{regen} \quad \forall \omega < 0 \end{cases} \quad \text{Equation 47}$$

This set of rules ensures maximum regeneration from braking at all times with no regard to state of charge. For the test platform this is unlikely to pose any problem since it is battery powered only and the likeliness for it going down a hill long enough to overcharge the batteries has to be regarded as slim. The brake blending strategy implemented corresponds to the series braking strategy presented in chapter 2.3.3.

4.3.3 SUS controller

The SUS controller presented in Figure 23 is a workaround that had to be implemented due to the built in controller in the SUS. The built in SUS controller takes a target speed as input variable, and returns current speed and current torque as feedback. A problem that became obvious early in the project was the properties of the built in controller. The motors showed behaviour with heavy wind-up. The control system in the SUS is believed to have a cascade structure where the speed controller is assumed to be a PI controller with a dominant integral part. Thus will the output from the motor be according to Equation 48 with K_p and K_i being unknown properties. Where $T(k)$ is the torque output of the motor at sample k and $\omega_{ref}(k)$ is the control signal.

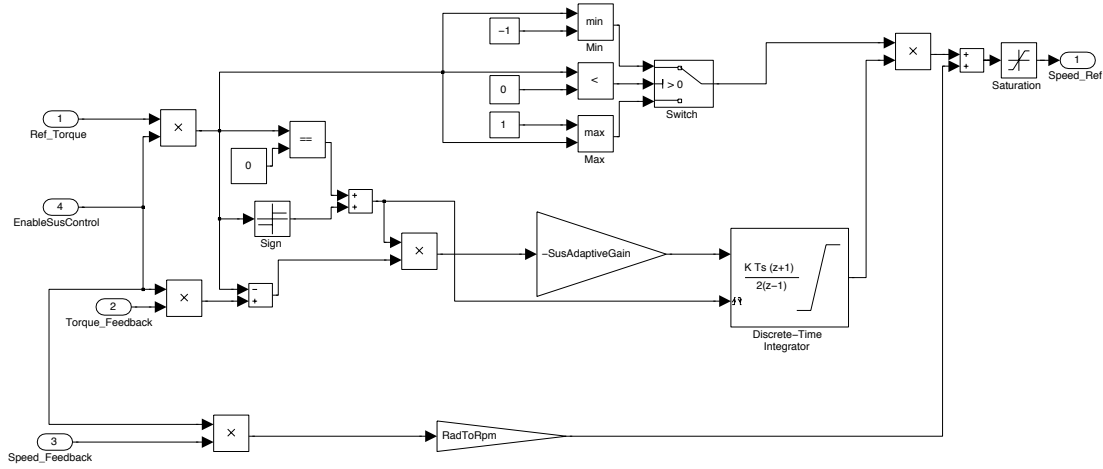


Figure 23: SUS controller in the wheel controller for the test platform.

$$T(k) = K_p (\omega_{ref}(k) - \omega(k)) + K_i \sum_{k=0}^k (\omega_{ref}(k) - \omega(k)) \quad \text{Equation 48}$$

The two main problems with the built in SUS controller is the unavoidable wind-up properties of a controller with a dominant integral part and that the reference signal is speed and the desired control property is torque.

If the previous sample of the speed is included in the reference speed it can effectively cancel out the error ($\omega_{ref} - \omega$) in the controller and thus the speed dependent output. Under the assumption that $\omega(k) \cong \omega(k-1)$ Equation 49 cancels out the speed dependency where u_1 is the reference torque and ω is the motor speed.

$$\omega_{ref}(k) = u_1(k) + \omega(k-1) \quad \text{Equation 49}$$

Then the motor torque output T becomes:

$$T(k) = K_p u_1(k) + K_i \sum_{k=0}^k u_1(k) \quad \text{Equation 50}$$

The PI-controller properties still affect the output but it is now possible to control the output based on torque feedback as the torque is decoupled from the speed feedback.

The optimum control signal would be a signal that cancels out the integral part, leaving only a proportional linear response. The inverse of the integral part of the controller would be an initial high output which then rapidly decreases. Since the built in controller was deemed to have a high-gain integral part and a low-gain proportional part, a very high control signal is required to get a rapid initial response. Since the gains K_p and K_i are unknown and could vary in time an adaptive approach was tried.

Several approaches were tested to achieve a control signal with the right shape and good tracking of the reference signal. The final controller is based on a modified MIT rule controller. But instead of the usual application of the MIT rule where the integral part adapts to slowly varying dynamic properties, a high gain that enables the output to change quickly was adopted. A high gain usually leads to an unstable controller but since the SUS controller integral part is dominant it is more tolerant for rapidly changing input signals than a normal PI-controller. The equation for the control signal is presented in *Equation 51* where u_2 is defined in *Equation 53* and K_r is an adaptive gain defined in *Equation 52*.

$$\omega_{ref}(k) = u_2(k)K_r(k) + \omega(k-1) \quad \text{Equation 51}$$

$$K_r(k) = \sum_{k=0}^k (u_1(k) - T(k-1))u_3(k) K_a \quad \text{Equation 52}$$

In *Equation 52* K_a is the tuning variable setting the response and rate of change of the adaptive gain and u_3 is defined in *Equation 54*. The variable u_2 is introduced instead of u_1 to be able to control the windup even under a zero torque request. This is necessary due to the feed forward structure of the controller, as a zero reference value would mean zero control signals.

$$u_2(k) = \begin{cases} u_1(k), & u_1(k) \leq -1, u_1(k) \geq 1 \\ 1 & 0 \leq u_1(k) < 1 \\ -1 & -1 < u_1(k) < 0 \end{cases} \quad \text{Equation 53}$$

The variable u_3 is a simple sign variable that is defined as one when u_1 is zero.

$$u_3(k) = \begin{cases} 1 & u_1(k) \geq 0 \\ -1 & u_1(k) < 0 \end{cases} \quad \text{Equation 54}$$

Thus the torque output from the motors at sample k , will be as in *Equation 55* with the controller output as defined in *Equation 51*. The key concept here is that K_p and K_i are still unknown but since the controller is adaptive it will track the reference torque given in u_1 .

$$T(k) = K_p u_2(k)K_r(k) + K_i \sum_{k=0}^k (u_2(k)K_r(k)) \quad \text{Equation 55}$$

4.3.4 Brake Controller

The brake controller which is shown in Figure 24 translates a torque request into a brake pressure request sent to the pump controller. The pump controller has for latency purposes been implemented directly in the PCU.

The brake controller is a feed forward adaptive controller to be able to handle wide range of friction coefficients for different temperature ranges. Since there's no feedback from the resulting braking torque on the wheels or the temperature, the controller runs a model of the disc brake to estimate the required brake pressure for a certain torque.

This could have been achieved with gain scheduling as well, but using an adaptive algorithm in this case is more of a time saving effort as tuning time is more or less diminished. One advantage of using an adaptive controller is that it makes it possible to exchange the brake model for an more advanced non-linear model in future revisions without retuning. The adaptive algorithm has been implemented using the MIT rule (Egardt 2008).

It is then used in a feed forward configuration, as the friction coefficient can be assumed to vary slowly during the course of the braking session. It is a suitable application of the MIT rule.

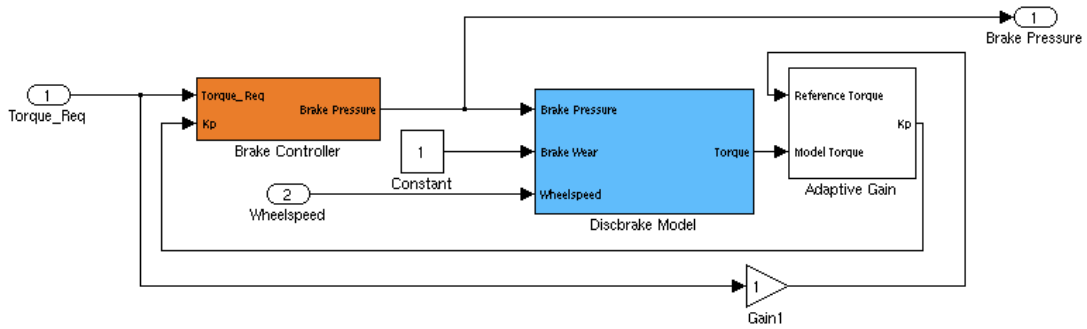


Figure 24: Brake controller in the wheel controller for the test platform.

The algorithm for varying the adaptive gain K_r is the following

$$K_r = -\gamma \int ((T_{\text{model}} - T_{\text{req}}) T_{\text{req}}) \quad \text{Equation 56}$$

where γ is the tuning coefficient, T_{model} is the model torque and T_{req} is the requested torque. The brake model used is the model defined in Equation 45. Equation 58 can be derived from the base form of the MIT rule if the criterion J is formed as in Equation 57 (Egardt 2008).

$$J(\theta) = \frac{1}{2} e^2(\theta) \quad \text{Equation 57}$$

The MIT-rule states that the parameters should be adjusted based on the negative gradient of the criterion J :

$$\dot{\theta}_i = -\gamma \frac{\partial J(\theta)}{\partial \theta_i} = -\gamma e \frac{\partial e(\theta)}{\partial \theta_i} \quad \text{Equation 58}$$

The gain parameter is $\gamma > 0$ and the derivative $\frac{\partial e(\theta)}{\partial \theta_i}$ is the sensitivity derivative. In our case $\theta_i = K_r$, by freezing K_r in time the assumption that $\frac{\partial e}{\partial K_r} = \frac{\partial y}{\partial K_r}$, where $e = (T_{model} - T_{req})$ and $y = T_{req}$ we can finally form the function as in *Equation 58* (Egardt 2008).

5 Implementation of test platform

5.1 System overview

To test the concept with a hybrid wheel loader with individual wheel motors a small scale test platform based on an articulated riding lawn mower was designed and built. A schematic overview of the test platform and a picture of it are shown in Figure 25 and Figure 26. The lawn mower's original internal combustion engine was removed and replaced with electrical motors on each wheel. A mechanical brake system was assembled on the test platform with brakes from a motorcycle and with a hydraulic unit (ESP-block), originally used in an ESP system (Electronic Stability Program) to control the brakes. The control system on the test platform consists of three ECUs, one that is running the vehicle control code, one that act as a gateway and the last ECU is an input/output node. The communication between the ECUs is CAN based. The test platform is equipped with a main switch, properly dimensioned fuses and an emergency stop for safety reasons. Two lead acid batteries deliver the energy to the platform.

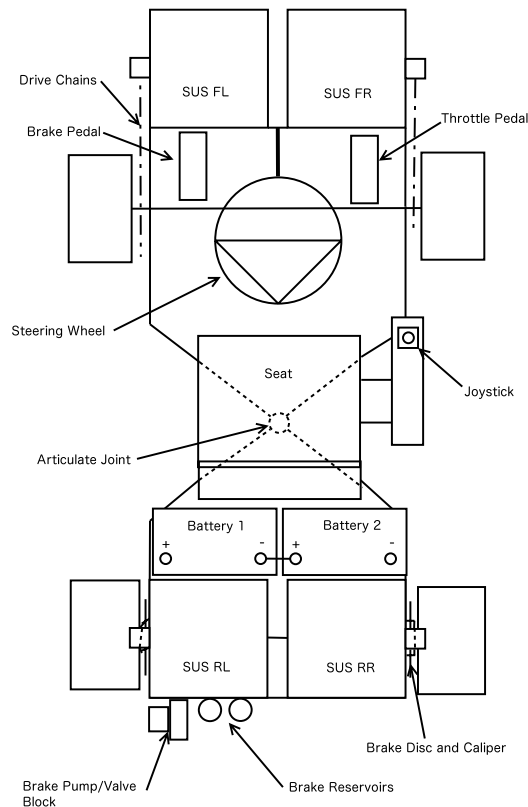


Figure 25: Overview of the test platform, with its main components.



Figure 26: The test platform designed and built in the project

5.2 Electric motors

The test platform is powered by four electrical machines called SUS which has a built in inverter and control system and the motor in the SUS is of PMSM type. The SUSes are mounted close to the wheels and the power transmission between the motor and the wheel is with a chain drive. The gearing between the motor and the wheel is 76:14. The SUSes are mounted in a way that allows the chain to be tensioned by sliding the SUS in the rear and put shims under the SUS in the front. The SUSes are connected to the CAN network on the test platform. The control signal sent to the SUS is a speed reference and as feedback the SUS gives the actual speed and actual torque. The output signals are updated every 100 ms. The tested torque and power performance of the SUS is presented in chapter 6 Results and Validation.

One of the constraints in the project was to use the SUS motors because they are a CPAC Systems product and they already have a CAN interface to the rest of the control system

5.3 Brakes

5.3.1 Brake discs and calipers

The brake discs and calipers are rear brakes from the Suzuki GSX-R series. With opposed two piston calipers and solid drilled discs. The discs are in a floating discs arrangement that differs from a normal car setup where the calipers themselves are floating. From a performance point of view it should not mean a significant

difference. The two piston configuration means that a higher braking force is achieved compared to a one piston configuration with the assumption that the area of the two pistons exceeds a comparable one piston caliper. The calipers are mounted as the lowest points in the system which design wise is a good choice as it is harder for air to get trapped in the calipers.

5.3.2 Pump

The pump is built into one unit together with the pressure control valves as an integrated hydraulic unit. As can be seen in Figure 27 the hydraulic unit is divided into two distinct hydraulic circuits. Each circuit has its own pump driven by a shared electric motor. In practice it means that it is not possible to run only one pump, both pumps always run at the same time. However the valve system can be set up in such a way that the pump does not build up brake pressure.

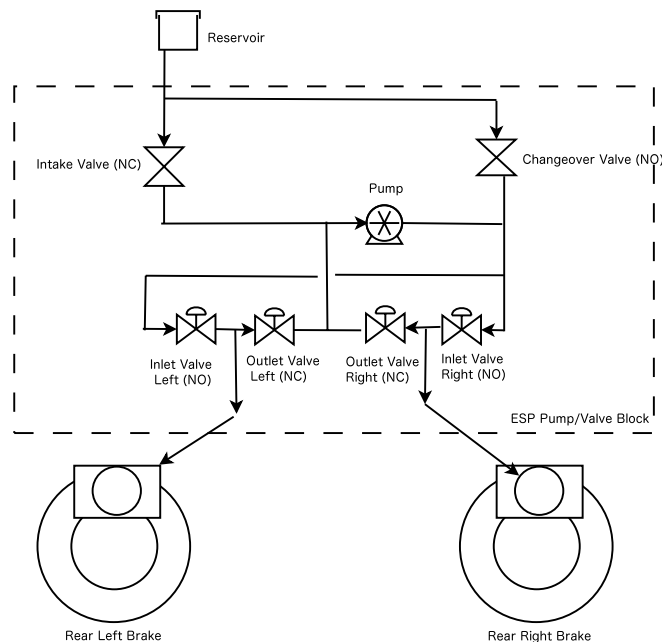


Figure 27: Schematic over the whole brake system and one circuit in the ESP-block.

5.3.3 Pressure control

The ESP-block consists of 12 valves with the following functions.

- Two changeover valves (one per circuit) which in the original automotive application is used to switch between manual and ESP brake operation. In this application they are energized when building pressure and are used to rapidly decrease the pressure in one circuit.
- Two intake valves (one per circuit), these valves switch the inflow to the pump from either scavenging fluid from the brake caliper side or pumping fluid from one of the reservoirs.
- Four inlet valves (one per caliper, two per circuit), normally open valves that can be closed to prevent pressure build up on one brake or closed to lock in a pressure.

- Four outlet valves, (one per caliper, two per circuit). Normally closed valves which in the original automotive application are used for the ABS functionality to quickly scavenge fluid to relieve the brake pressure rapidly. In this application this valve is used to modulate the pressure by controlling the valve with a PWM signal.

The pressure control is done through a feedback loop using a brake pressure sensor. The ideal setup would be to use one pressure sensor per wheel and that would enable to run almost fully individually controlled brake pressures. It is also possible, however, to run the brakes per circuit using one pressure sensor per brake circuit. This does take away the possibility to individually control the brakes from left to right but it also results in a big simplification of the control algorithms. Due to time constraints and physical constraints only the rear circuits were implemented on the test platform. The control of the brakes is also implemented in its simplest setup by controlling the brakes as a pair with one brake pressure sensor.

The control algorithm implemented is a non linear PI controller which is shown in Figure 28. The nonlinearity consists of Gain scheduling as the dynamics of the system is heavily dependent on the brake pressure. A lot of manual tuning effort went into the controller as the dynamics were hard to predict. One uncertainty could be microscopic air bubbles in the system which leads to that the initial response is very different compared to the response when the bubbles have been compressed.

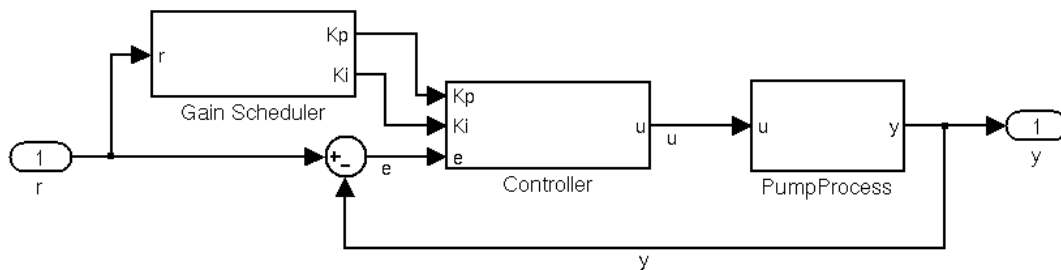


Figure 28: Control structure for brake pressure control on the test platform.

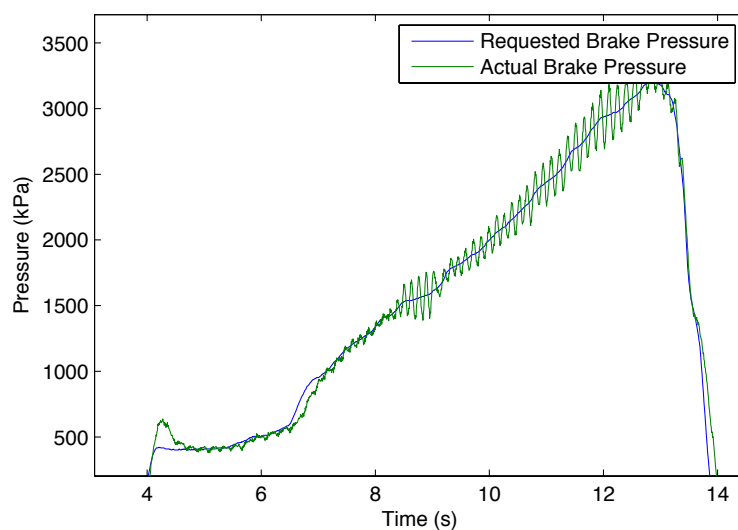


Figure 29: Test of brake pressure controller.

In Figure 29 a test run is done with gradually increasing brake pressure reference value. During testing it turned out that the lower brake pressure limit for this configuration was approximately 300kPa. The pressure follows the reference up to 3500kPa with slight oscillations. The tuning was limited to return a good result up to 3500kPa as the brakes at that pressure delivers a braking torque high enough to lock up the wheels at speed. The pump however is able to deliver pressures in excess of 25000kPa where the pressure sensor saturates. A software cut-out opening the changeover valve has been implemented at a controller level on 15000kPa to protect the hydraulic components from bursting from overpressure.

5.4 Electric power and wiring

The main electrical system on the lawn mower is a 24V system based on two 12V lead acid AGM batteries connected in series. From one of the batteries a 12V power supply is taken. This makes the batteries unbalanced because the power drain from the batteries is not equal. Charging the batteries individually solves the unbalancing problem.

Both the 24V and 12V system can be disconnected by an emergency stop relay actuated by an emergency stop button. A main switch turns off both systems. All loads are properly fused.

A full electric power supply schematic can be found in Appendix 3: Electric power supply schematic for the test platform.

5.5 Network, sensors and data logging

The main hardware parts in the control system on the test platform is a ECU handling the vehicle control (FAF), a ECU that works as a gateway (HCU) and a ECU that handles physical in- and outputs (PCU).

The FAF processor is a floating point processor and it runs the model that controls the test vehicle. The code in the model is generated with a code generation tool from MATLAB/Simulink.

The HCU is the gateway in the system and it handles the data from the FAF, the battery sensor bus, the joystick and steering resolver bus and the CAN-bus where the PCU and the SUSes are connected.

The PCU is an input/output node and it controls the valves and the pump in the ESP-block and it reads the signals from the brake pressure sensor, the throttle pedal and the brake pedal.

A full schematic of the communication and the signals can be found in Appendix 4: Communication and signal overview for the test platform.

The function calls in the FAF, HCU and PCU code can be scheduled to run every 8 ms, 16 ms, 32 ms or 256 ms. The main vehicle control model is executed every 8 ms which is the fastest possible. The execution time for the sensor inputs, actuator outputs and the gateway is set to not overload the processors in respective ECU and the CAN busses. The delay for inputs, outputs and the gateway is presented in *Table 1*. All signals on the lawnmower CAN bus are available for logging and the log files can be processed in MATLAB.

Table 1: Signals to and from the FAF and their total delay.

	PCU	SUS	HCU	FAF	Max total sample time
Inputs PCU					
Brake pedal position	8ms		8ms	8ms	PCU-->FAF: 24ms
Throttle pedal position	8ms		8ms	8ms	PCU-->FAF: 24ms
Brake pressure rear brakes	8ms		8ms	8ms	PCU-->FAF: 24ms
Inputs Battery sensor					
Battery current			16ms	8ms	HCU-->FAF: 24ms
Battery voltage			16ms	8ms	HCU-->FAF: 24ms
Battery temperature			16ms	8ms	HCU-->FAF: 24ms
Inputs Joystick/Steering wheel					
Steering wheel angle			8ms	8ms	HCU-->FAF: 16ms
Joystick			16ms	8ms	HCU-->FAF: 24ms
Inputs SUS					
SUS rear right actual speed		100ms	8ms	8ms	SUS-->FAF: 116ms
SUS rear right actual torque		100ms	8ms	8ms	SUS-->FAF: 116ms
SUS rear left actual speed		100ms	8ms	8ms	SUS-->FAF: 116ms
SUS rear left actual torque		100ms	8ms	8ms	SUS-->FAF: 116ms
SUS front right actual speed		100ms	8ms	8ms	SUS-->FAF: 116ms
SUS front right actual torque		100ms	8ms	8ms	SUS-->FAF: 116ms
SUS front left actual speed		100ms	8ms	8ms	SUS-->FAF: 116ms
SUS front left actual torque		100ms	8ms	8ms	SUS-->FAF: 116ms
Vehicle steering angle actual		100ms	8ms	8ms	SUS-->FAF: 116ms
Outputs PCU					
Req brake pressure rear right	8ms		8ms	8ms	FAF-->PCU: 24ms
Req brake pressure rear left	8ms		8ms	8ms	FAF-->PCU: 24ms
Outputs SUS					
SUS rear right requested speed		?	16ms	8ms	FAF-->SUS:
SUS rear left requested speed		?	16ms	8ms	FAF-->SUS:
SUS front right requested speed		?	16ms	8ms	FAF-->SUS:
SUS front left requested speed		?	16ms	8ms	FAF-->SUS:

5.6 Controller Implementation

5.6.1 Implementation method

The implementation of the controller was done in Simulink and Stateflow with the code generation tool TargetLink. Using TargetLink meant that some parts of the model and controller structure had to be adapted according to the TargetLink modelling guidelines. The TargetLink guidelines are strict in terms of which blocks that are allowed and how the model should be structured (dSPACE 2010). TargetLink offers a wide range of optimizations for different processor architectures etc, but since a powerful floating point PPC processor was used in the project generic C floating-point code could be generated and used successfully. TargetLink generated a main controller function and supporting functions. This function was in turn called every 8 ms from the real time OS running on the processor. The process for implementing the control strategy is shown in Figure 30.



Figure 30: Overview of implementation of control strategy.

5.6.2 Implementation in vehicle

The initial implementation workflow was on the basis test and tune, and very much an iterative process. An example of this process was a major retuning that had to be done due to unexpected delays in the system. The feedback from the electric motors was only updated every 100 ms with a 100 ms delay. As the controller was designed for getting feedback every 20 ms with little to no delay the resulting functionality was poor. The delay was implemented in the vehicle model and the controller modified. The typical workflow which is also shown in Figure 31 was Model → Test → Evaluate → Remodel.

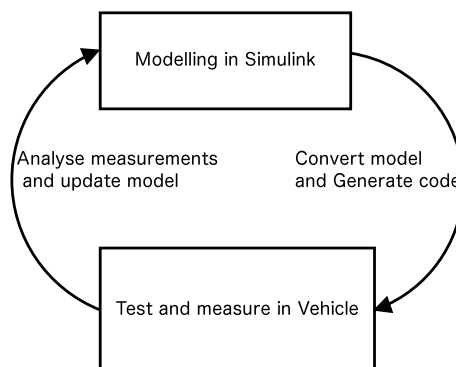


Figure 31: Implementation workflow.

5.6.3 Data analysis and measurements

For logging data the main CAN bus was used in conjunction with a PC-CAN interface to sniff the data on the bus. The raw log files were then parsed with scripts written in MATLAB to structure and visualize the vehicle data. This enabled very rapid data analysis of the vehicle behaviour enabling a fast development pace.

6 Results and Validation

In this chapter test results and validation of models for the electric motors, the brakes and the vehicle control will be presented.

6.1 Electric motor validation

Both parts of and the full SUS (electric motor) model was validated from test on the SUS with the wheels running individual in the air and with the SUSes powering the test vehicle. The tests first followed a test plan attached in *Appendix 5: Test plan and verification of SUS* to validate the parameters in the SUS. Because of noisy signals, mechanical problems and that it was hard to control the brake pressure exactly the test plan was revised to tests that was better adapted to the conditions.

With the test setups the following parameters were measured or validated:

- The maximum and the minimum torque as a function of the speed
- The power consumption
- The relationship between speed reference and torque output

During the tests it was assumed that the actual torque followed the internal SUS torque request very fast and therefore it was assumed that the reference torque was equal to the actual torque all the time. *Please note that the SUSes used are prototype versions and do not reflect the performance of the production units.*

6.1.1 SUS torque as a function of speed

To measure the maximum and the minimum torque as a function of the speed for the SUS the test setup was to accelerate and decelerate with the SUS to its performance limit. This was done with two tests

- With the wheels in the air accelerate the wheel to the maximum speed and while keeping a full speed request braking the wheels to stand still with the mechanical brakes. With this test only the accelerating performance of the SUS was tested. (Corresponds to test case A in the revised test plan in *Appendix 5: Test plan and verification of SUS*)
- With the test vehicle running on the ground accelerate the vehicle as fast as possible to a safe speed and then decelerate with maximum electric braking torque. With this test both the accelerating and deceleration performance of the SUS was tested. Compared to testing the SUS with the wheel in the air it was not possible to test to as high speeds because the vehicle speed would have been too high. (Corresponds to test case B in the revised test plan in *Appendix 5: Test plan and verification of SUS*)

From these tests the logged speed vs. torque points were plotted and the maximum acceleration and deceleration could be found as the outer points in the graph. The maximum torque for acceleration was measured up to 3000 rpm and for the deceleration the torque was measured up to 1100 rpm. The result from the test can be found in Figure 32. From the measured maximum SUS-torque a speed vs. power curve could be calculated from Equation 6 which can be found in Figure 33. The

measured maximum speed vs. torque curve was used in the SUS model as a torque limit.

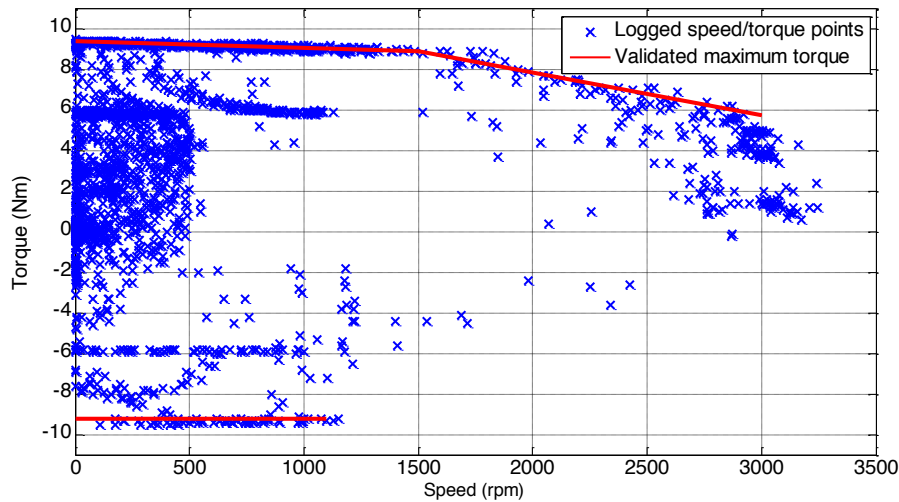


Figure 32: Speed vs. torque test for the SUS and measured maximum speed vs. torque curve.

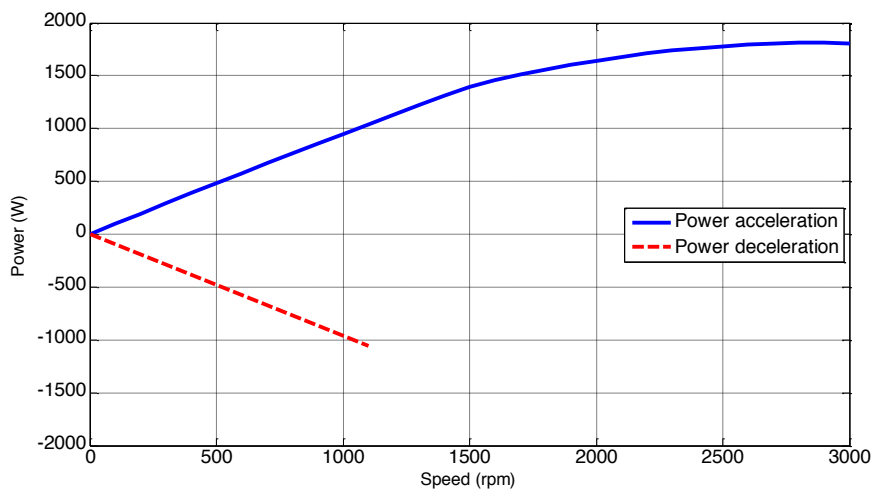


Figure 33: Speed vs. power curve for SUS during acceleration and deceleration.

6.1.2 Electric power consumption for SUS and all other consumers

From the electric power consumption test the power consumption of the ESP block, the idle power for the SUS and the efficiency of the converters and the electric motor in the SUS could be found. The ESP-block power and the SUS idle power could be found directly from logged data and the efficiency was tuned until the simulated and logged data was the same with the same torque request and speed on the SUS. From logged data it could be seen that the average idle power for three SUSes is 82 W and when the brake pump is running the average power consumption is 470 W. An example of power consumption when the SUSes are in idle and when the brake pump is running can be found in Figure 34. The efficiency in the converters and the electric motor was found to be 90 % and the simulated electric power consumption compared

with measured electrical power consumption can be found in Figure 35 and Figure 36. A compilation of the electric power parameters can be found in Table 2 below.

Table 2: Power consumption parameters for test platform.

SUS idle power	27,4W
ESP-block active power	390W
SUS converter efficiency	90%

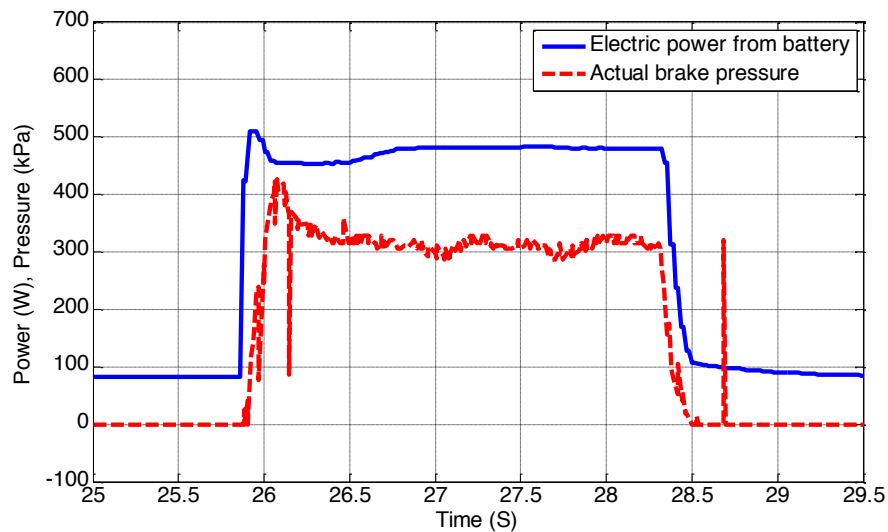


Figure 34: Electrical power from the battery and actual brake pressure

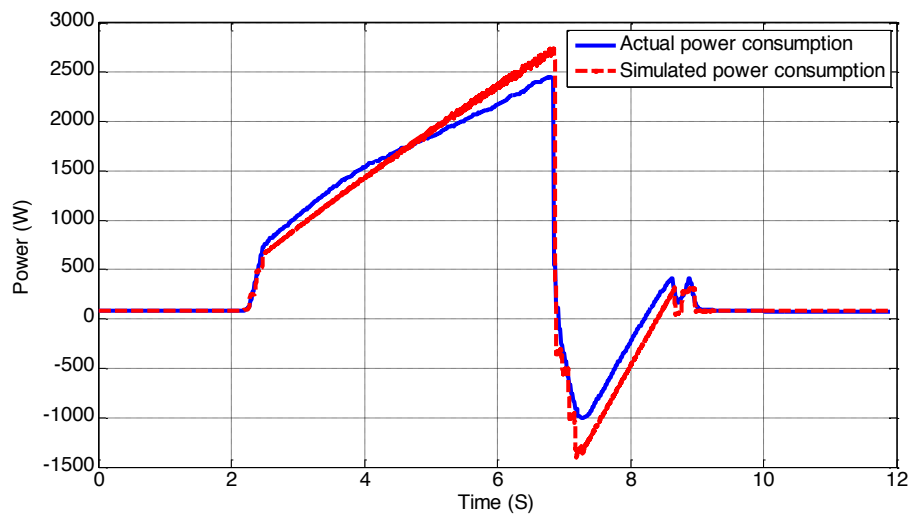


Figure 35: Actual and simulated power consumption during test run with the test platform

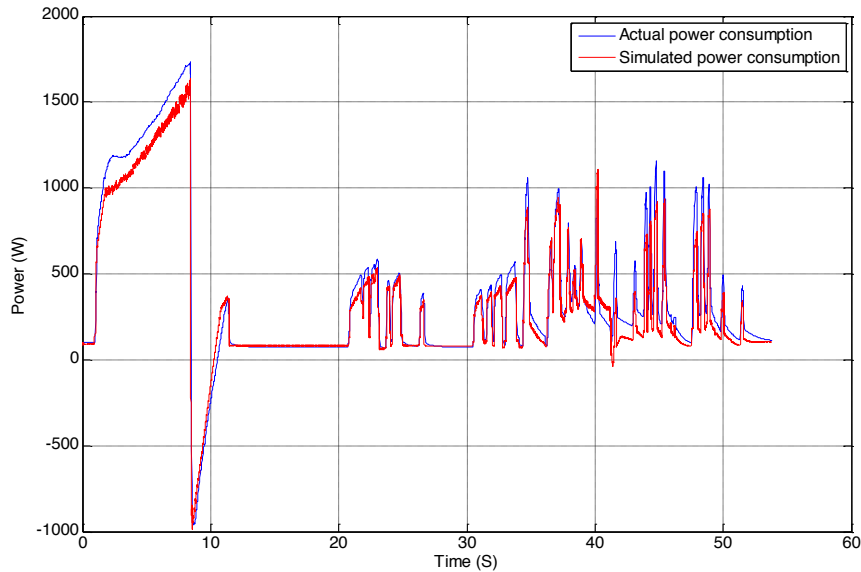


Figure 36: Actual and simulated power consumption during test run with the test platform

6.1.3 SUS speed controller

To estimate the controller parameters in the speed controller in the SUS a number of different test runs were carried out to gather data. When finding the parameters in the SUS controller it was assumed that the requested torque inside the SUS was the same as the actual logged torque. This assumption was made because the electrical characteristics are much faster than the mechanical characteristics. The test setup for the speed controller can be found in *Appendix 2: Model used for verification of SUS speed control parameters*. The parameters in the controller were tuned until the simulated torque reference out from the controller followed the logged torque reference. An example of comparison between simulated and logged data can be found in Figure 37. The difference between the actual and the simulated torque in the plot between 14 and 20 seconds depends on that the data comes from a driving test with the test platform and when the test platform was stopped there was still a torque on the electric motor but it was not big enough to get the test platform running.

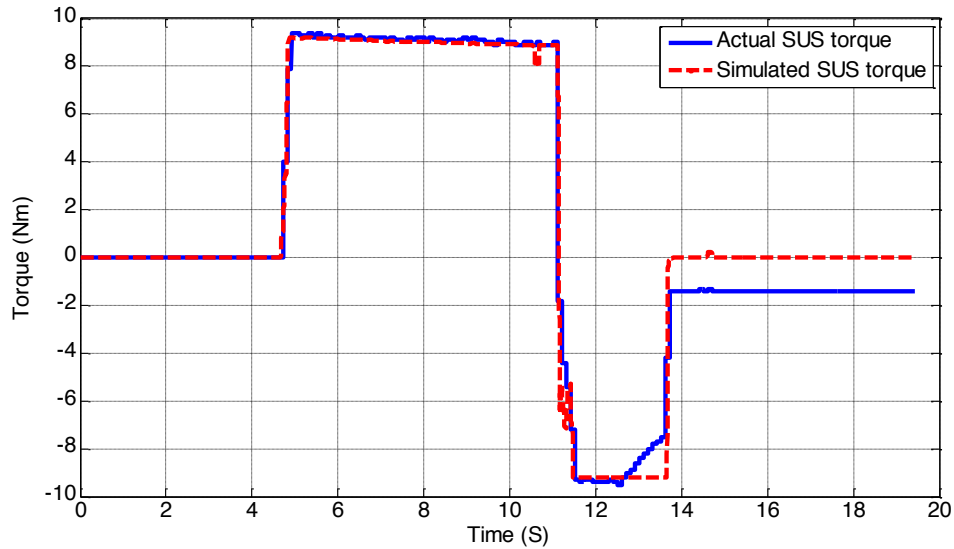


Figure 37: Actual and simulated torque from SUS from a driving cycle with first maximum acceleration and after that maximum deceleration.

6.1.4 Complete SUS model verification

The complete SUS model was verified against different driving cases with the test platform. The actual logged speed request to the SUS during driving was used as input to the SUS and vehicle models. For comparison the simulated speed and torque was compared with the logged torque. Example of verification between simulated and logged values can be found in Figure 38.

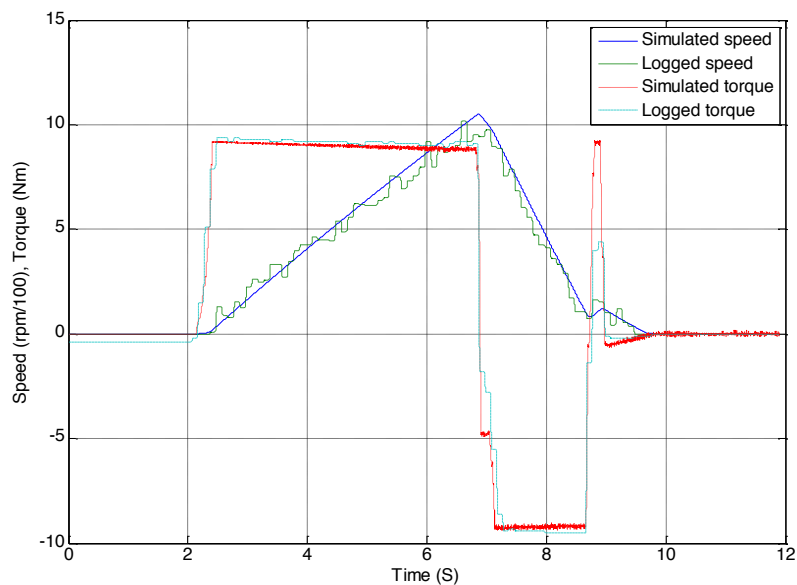


Figure 38: Simulated and logged speed and torque from a test run.

6.2 Brake validation

Validation of the brakes was done using the torque and speed measurement in the electric motors. With the wheels raised up from the ground the motors were accelerated to a given speed. Then brake pressure was gradually applied while the torque needed to keep the wheels spinning was measured. The brake pressure was monitored and logged to be able to use it as input to the brake model. The logged data was thereafter compared with the brake model output based on the logged brake pressure. The logged data from the test can be found in Figure 39.

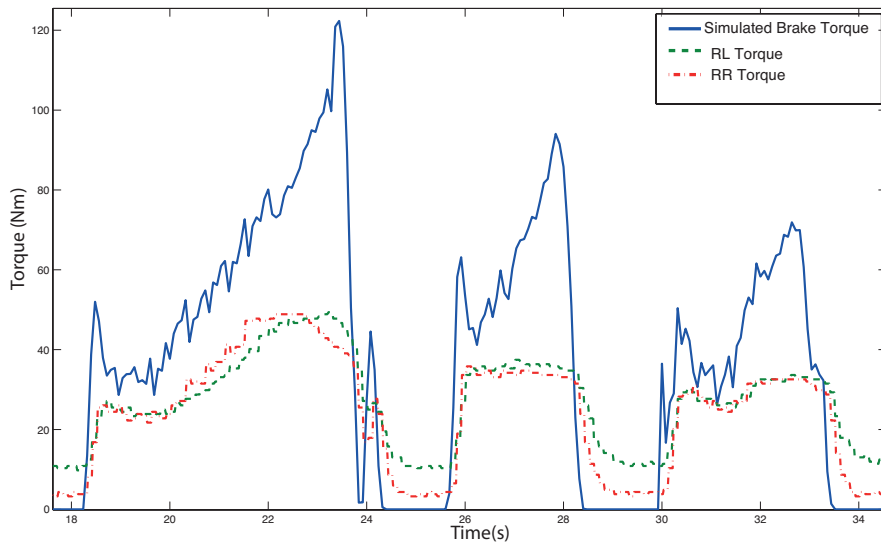


Figure 39: Measured brake torque on right and left wheel plotted against simulated torque on the unadjusted model.

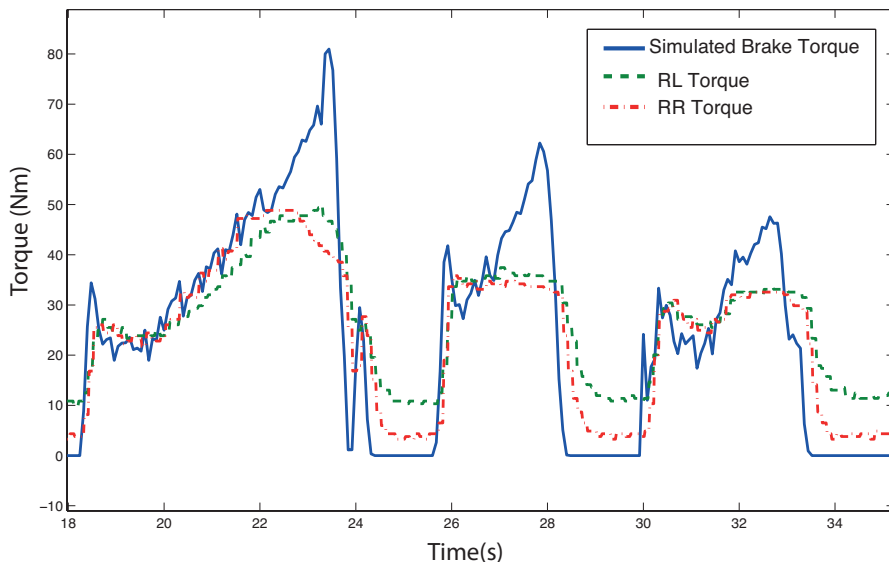


Figure 40: Adjusted brake model with lowered friction coefficients.

The brake model was adjusted by lowering the friction coefficient of the brake pads. The discrepancies in the model vs. the real world could have several reasons. The brake calipers and disc are salvaged parts from a junkyard showing a lot of wear and

tear and the specific friction material properties are unknown. The logged data from the test with adjusted brake parameters can be found in Figure 40.

As can be seen in the measurement graphs the motor torque is limited. Up to the maximum torque of the motors the adjusted model correlates reasonably well with the measurements. Based on the acceptable correlation in the measurable range, the assumption has been made that the brake model is true also for higher brake pressures. This is motivated by the fact that the brake model is fully linear to the brake pressure.

6.3 Control validation

The benchmark for how well the control design performs is in the end the driver experience. Driving experience is a very subjective measure and varies from person to person, but with certain key concepts that are necessary for driver confidence. These key attributes are consistent and easily controlled behavior. They are essentially that the vehicle should respond on user input in similar fashion at all times and that it is possible to modulate output easily.

6.3.1 Brake blending

At the start of the project the brake blending was the main focus i.e. achieving a good transparent brake blending with energy recovery. Since the thesis evolved into developing a functional test platform, the amount of time evaluating brake blending decreased. A well functioning brake blending system was however designed and tested at moderate speeds (below 16 kilometers per hour).

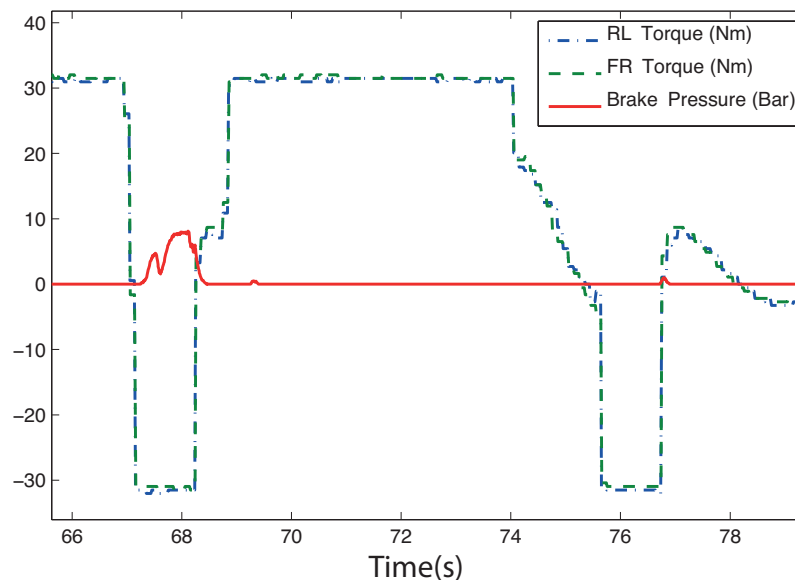


Figure 41: Two braking cycles measured on the test platform, first with blended braking and followed by a pure electric braking cycle.

In Figure 41 two braking scenarios can be seen. In the first braking scenario the braking request is above the maximum braking torque of the motors and the mechanical brakes are activated. In the second braking phase the braking request is set just below the saturation level and the mechanical brakes are not activated.

The brake-blending algorithm worked as expected, there was however initial problems in modulating the braking effort from a driver point of view. Often it resulted in too heavy braking action with locked wheels as a result.

The problem was deemed to have two main reasons, where the first one was the lack of feedback in the brake pedal to the driver. In a traditional braking system the driver gets feedback as the pedal stiffens when the brake pressure rises, whereas the brake pedal in this application is just spring loaded. The only driver feedback is thus the retardation of the vehicle, but as the brake pump does have a startup delay before it starts to build pressure, the initial feedback from pressing the brake pedal is missing which is the second reason it's hard to modulate the braking force.

Two solutions to this problem was considered either to predict when the pump is needed by activating it when the electric motors are close to their limit or to implement a rate limiter, limiting how fast the brake pressure can rise. Due to time-constraints only the latter one was tested and implemented successfully. In Figure 42 a test is conducted with a steady brake request and the rate limiter can clearly be seen on the brake pressure rise. It does impose further time delays but with limited speeds of the vehicle the result is satisfactory and drivability is good. For further development and higher operating speeds pre-emptive brake pump operation is recommended to be investigated further.

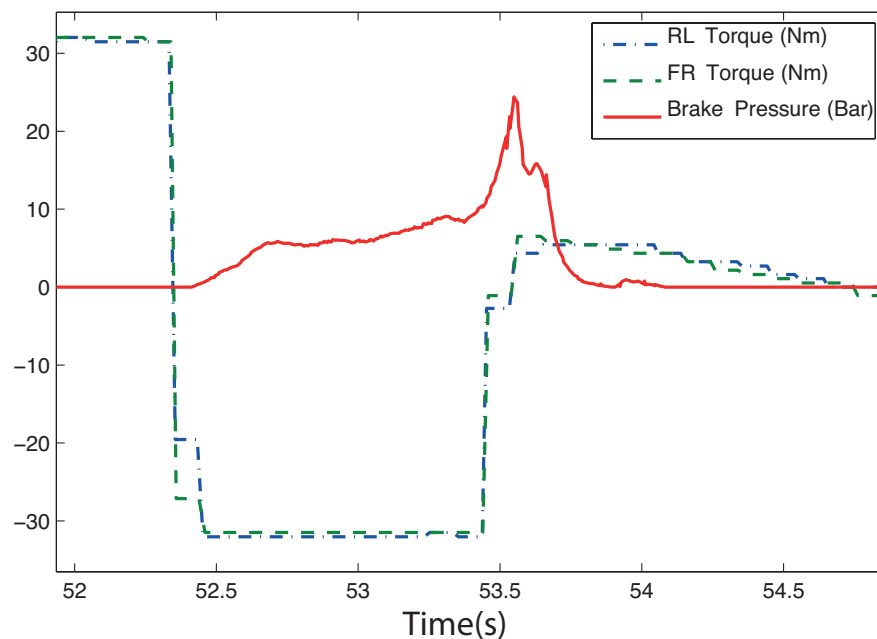


Figure 42: The rate limiter can be observed between 52.5 and 52.8 seconds limiting the brake pressure rise. At 53.4 seconds the vehicle is at a complete stop and a rapid pressure rise can be observed. When the controller goes into parking state the pressure is held to kill eventual remaining wind-up in the motors.

6.3.2 Controller behavior

The ability to control the torque of the motors is a key factor for the whole controller to function. In Figure 43 a run was logged with a step response to approximately 60% of full torque and then held for 5 seconds until gradually lifting off the gas pedal. There is a pronounced overshoot followed by oscillations around the reference point. A trade off between controller response and overshoot had to be made, and from a driver experience point of view response was deemed to be the most valuable property.

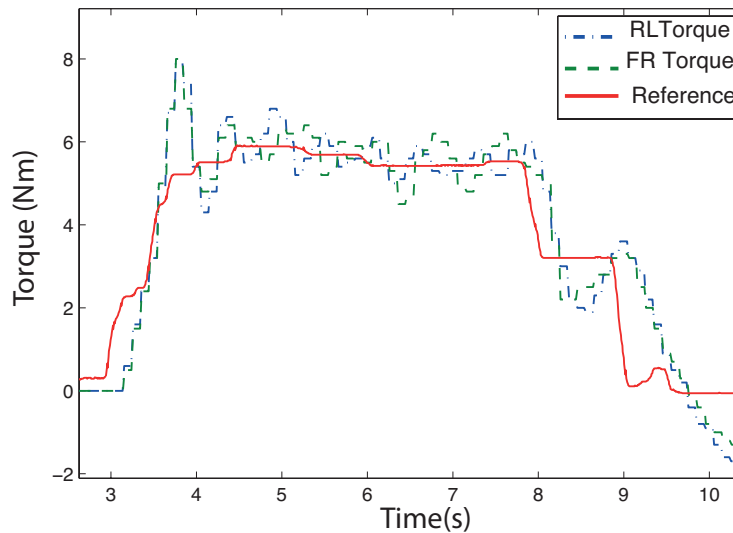


Figure 43: Reference torque tracking while holding a steady torque request.

When rapidly alternating the torque request as in Figure 44 and thus “stressing” the controller, the delay in the feedback can easily be seen.

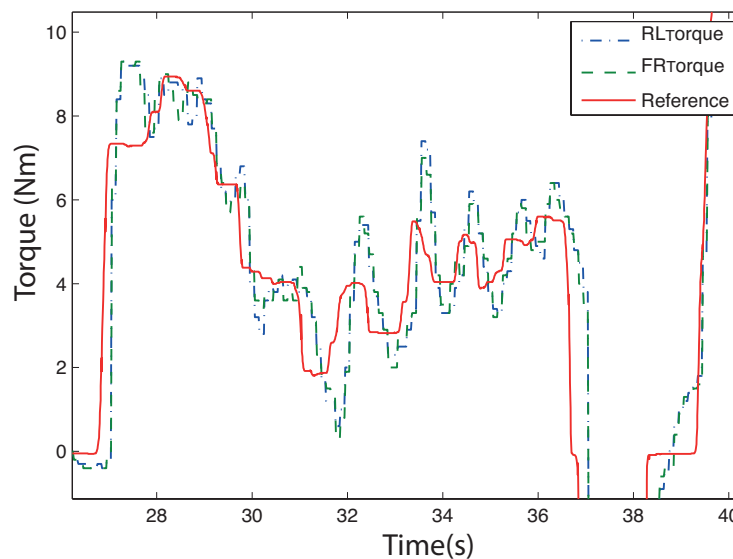


Figure 44: Reference torque tracking while rapidly changing the request.

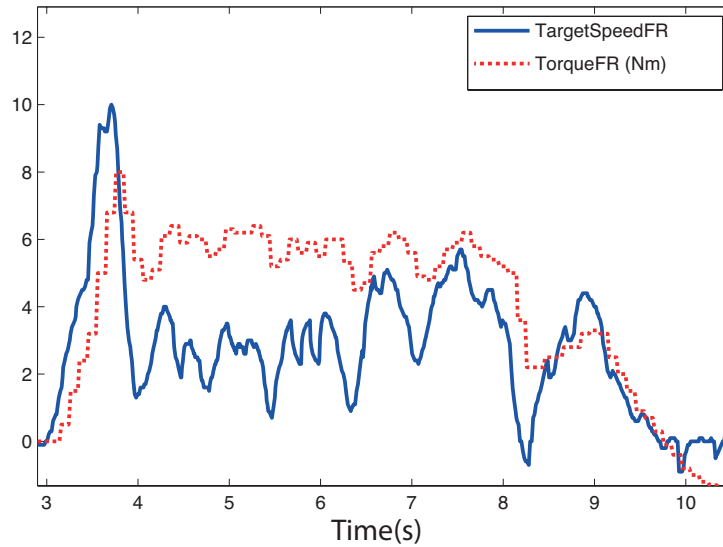


Figure 45: Input signal (*TargetSpeed*) and torque output for the steady reference signal shown in Figure 43.

As can be seen in Figure 45 the SUS controller sends a high control signal in the beginning, this is to stimulate the low gain proportional part in the internal SUS controller. This is followed by lowering the control signal to a semi steady state mode once the integral part of the controller had time to rise. As can be observed the control signal is anything else but smooth. Again, this is in effect a tradeoff between response and smooth control signals. But as the internal SUS controller has a dominant integral action the bumpy control signal is somewhat smoothed out before affecting the output. The same behavior is shown in the test region with an alternating reference signal in Figure 46.

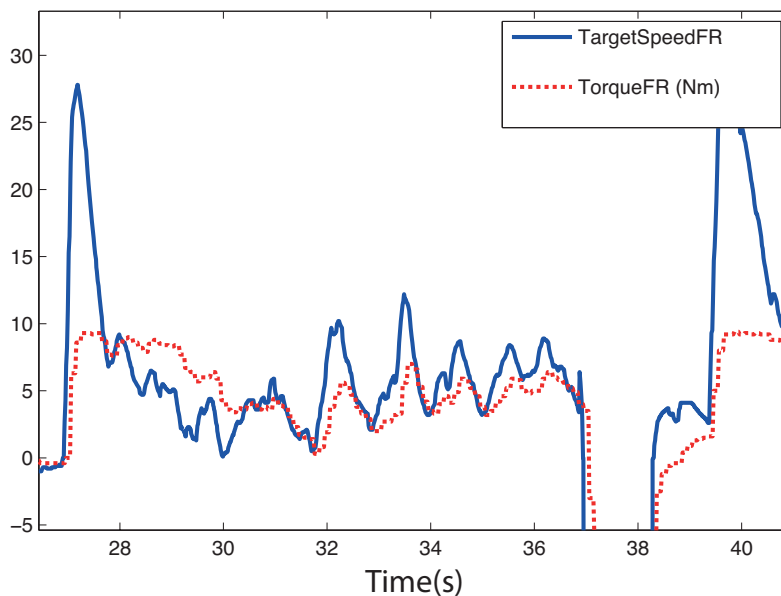


Figure 46: Input signal (*TargetSpeed*) and torque output in the same test region as in Figure 44.

7 Discussion

The test platform that was designed and built during the thesis project shall represent a full size wheel-loader in several aspects, as the goals set initially for the project put an emphasis on the scalability; this is arguably the most interesting property. In terms of physical layout with the articulate joint and individual wheel-motors the representation is very accurate with the exception of the lifting arm and bucket.

The intended use is for functional development of a hybrid drivetrain, which it is arguably suitable for. This is due to the physical properties but also due to the architecture of the electrical system on the vehicle. The principle of a vehicle network with actuator and sensor data enables both extensive data logging functionality as well as expandability by adding more nodes to the network. By designing the control using “Model based development” and automatic code generation the development time for the control and software became short.

7.1 Components

The components used for the test platform have been a mix of in-house, supplier and external components and all of them have posed different challenges. The in-house components have been the easiest to work with since all documentation are available together with extensive know-how. The electric motors which were a supplier component posed a different challenge as we were given an interface with predefined input and output variables but had no control over the software. This meant that the behavior of the electric motors first had to be benchmarked and analyzed and after that a control strategy suitable for our application had to be implemented outside the electric motors. To not have full control of the electric motors with effects as delays and windup at low speeds arguably makes the electric motors the weakest link in the test platform.

The external component used was the brake pump and valve block (ESP block), taken from a scrapped early 2000s Citroën. There was little to no documentation available and the original CAN bus interface used a non-published signal specification. The solution for the problem was a total reverse engineering where all electronics in the original ESP block was bypassed and the control for the pump and the valves in the ESP block was moved to an in-house ECU. This was very time consuming but combined with the in-house ECU, good functionality could be achieved. The current solution have the constraint of only braking one axle, and not being able individually braking the wheels. But it is solely due to time constraints as the original ESP block can deliver full individual braking.

7.2 Testing and validation

The component models for the electric motors and the brakes that were used in the project were tuned through testing to make them sufficiently good for the vehicle control design. When comparing the simulated and the logged test values for the models the outputs are almost the same even if there are exceptions. Given the uncertainties such as the parameters in the built in electric motor controller, not verified test equipment and unknown components (e.g. the ESP block) the models are good. The validation of the models was presented in chapter 6.

Brake blending which was the second objective of the thesis was implemented and tested. The function that was achieved can be deemed satisfactory as it blends the brake effectively and does not lock the wheels. It is somewhat limited as brakes only were implemented on the rear axle which means that the braking force is relatively low when wheel-lock occurs. To maximize the possible braking action on the rear axle without lock-up the test platform only the rear motors were used during testing. This was done to limit the weight transfer to the front axle. It proves that the principle of brake blending does work but to make a real conclusion also front brakes have to be included.

In terms of drivability the platform behaves very well with throttle and brake pedal input. This could arguably be the biggest achievement in the scope of the thesis given the constraints on the motor control and the limited time frame.

8 Further Work

The main goal when designing and building the test platform was to be able to test functions in a smaller scale than on a full size hybrid wheel loader. In the main project towards the hybrid wheel loader there is a lot of further work, but this chapter will focus on further work towards the test platform.

The test platform is currently missing mechanical brakes in the front and it is not possible to control the brakes individually. If the current brake solution with the ESP-block should be used, the ESP-block has to be changed because one of the hydraulic circuits in the block is broken. To be able to control the brakes individually a new algorithm for controlling the valves in the ESP-block also has to be developed.

In the test platform's current state it would be possible to test other systems that is not that time critical, examples of such systems could be steer-by-wire for an articulated vehicle and to add a vision system to implement autonomous driving and safety features. For these tests only limited mechanical changes has to be made. The biggest mechanical update would be to mount a steering cylinder in the articulated joint on the test platform to add stability.

If the delays can be shortened and the signal quality improved in the system, even more time critical systems can be tested. Examples of that kind of systems could be a traction control system and ABS-brakes. The first component to replace or update in this case would be the SUSEs which have both long time delays in the signals and the signals are noisy.

Another test possibility on the test platform would be to change the batteries to a more advanced battery chemistry.

For the brake blending function it would be interesting to further look into how to balance the regeneration peak power and battery/capacitor charging levels towards the lifespan of the batteries/capacitors and other components in the system. For the driver interpretation of the brake by wire system some kind of feedback in the brake pedal could be implemented, e.g. a correlation between applied brake torque and how hard it is to push the brake pedal.

9 References

dSPACE GmbH (2010), *Modeling Guidelines for MATLAB/Simulink/Stateflow and TargetLink ver 3.0*.

Egardt B (2008), *Nonlinear and Adaptive Control, Supplement ESS076*. Chalmers University of Technology.

Frank P. Incropera, DeWitt, Bergman, Lavine (2007), *Fundamentals of Heat and Mass Transfer*. John Wiley & Sons, New York, USA

Harnefors L. (2002): *Control of Variable-Speed Drives*. Mälardalen University, Västerås, Sweden

Hughes A. (2006): *Electric Motors and Drives*. Elsevier, Oxford, Great Britain

Madås D, Lai H (2011), *Test Vehicle for Regenerative Braking Emulation*. Diploma work. Department of Applied Mechanics, Chalmers University of Technology

Mohan N., Undeland T., Robbins W. (2003): *Power Electronics Converters*, Wiley, Hoboken, New Jersey, USA

Mägi M, Melkersson K (2008), *Lärobok i maskinelement*. EcoDev Internatinal, Göteborg, Sweden

Niels J. Schouten, Mutasim A. Salman, and Naim A. Kheir (2002), *Fuzzy Logic Control for Parallel Hybrid Vehicles*, IEEE TRANSACTIONS ON CONTROL SYSTEMS TECHNOLOGY, VOL. 10, NO. 3, May 2002

Ostermeyer G.P, Müller M (2005), *Dynamic interaction of friction and surface topography in brake systems*. Institute of Dynamics and Vibrations, Technical University Braunschweig

Shuang Y, JunzhicZ, Lifang W (2009): *Power Management Strategy with Regenerative Braking For Fuel Cell Hybrid Electric Vehicle*, *Power and Energy Engineering Conference*; 28-31 March 2009, Wuhan, China. s.1-4.

Voller G.P., Tirovic M., Morris R., Gibbens P. (2003), *Analysis of automotive disc brake cooling characteristics*. Proceedings of the Institution of Mechanical Engineers, Part D: Journal of Automobile Engineering

10 Appendix 1: SUS models

Both the simple and the full electric motor consists of a speed controller, a current controller, the electrical part of the motor and the mechanical part of the motor together with the load. The model blocks are presented below.

10.1 Full SUS model

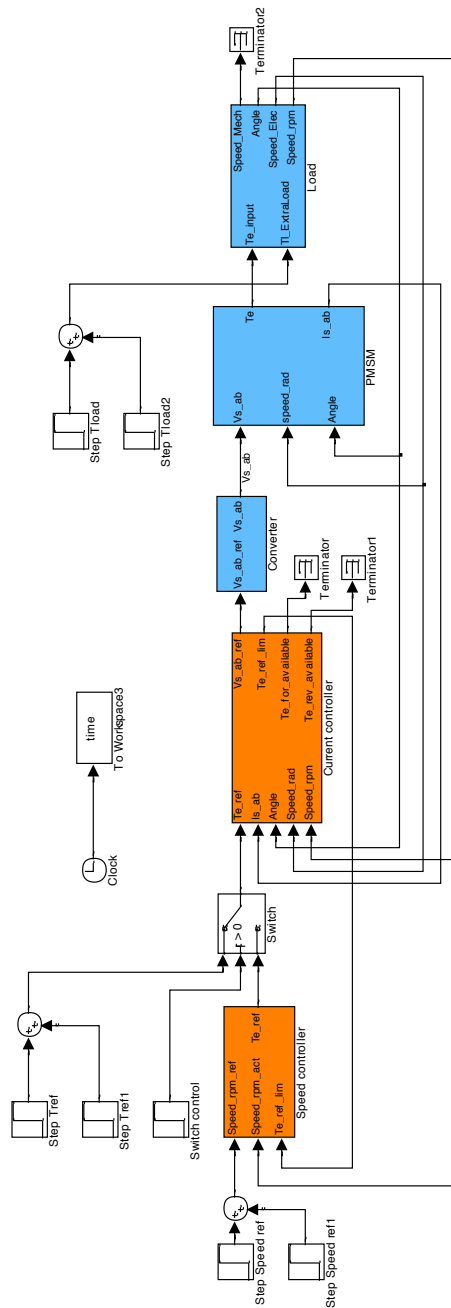


Figure: Overview of full SUS model

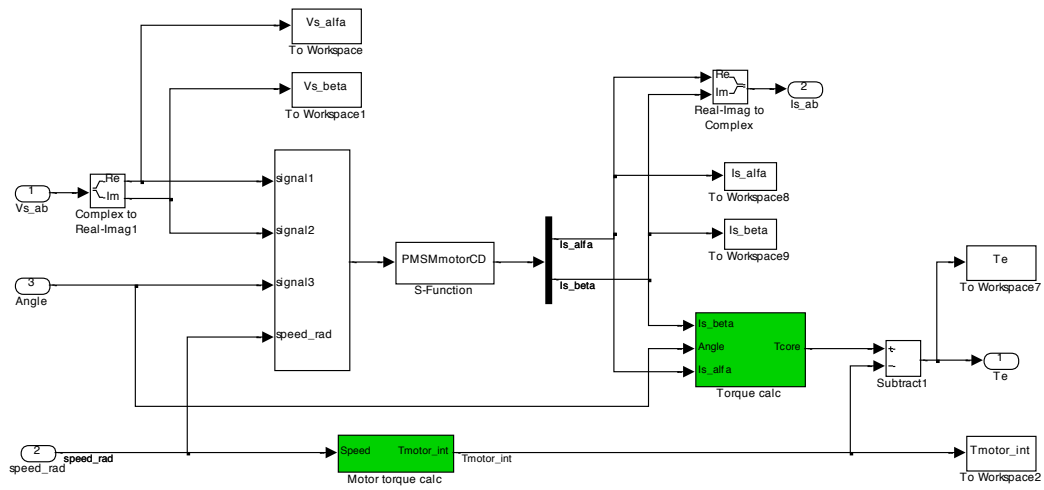


Figure: Electrical parts in full SUS model

10.2 Simple SUS model

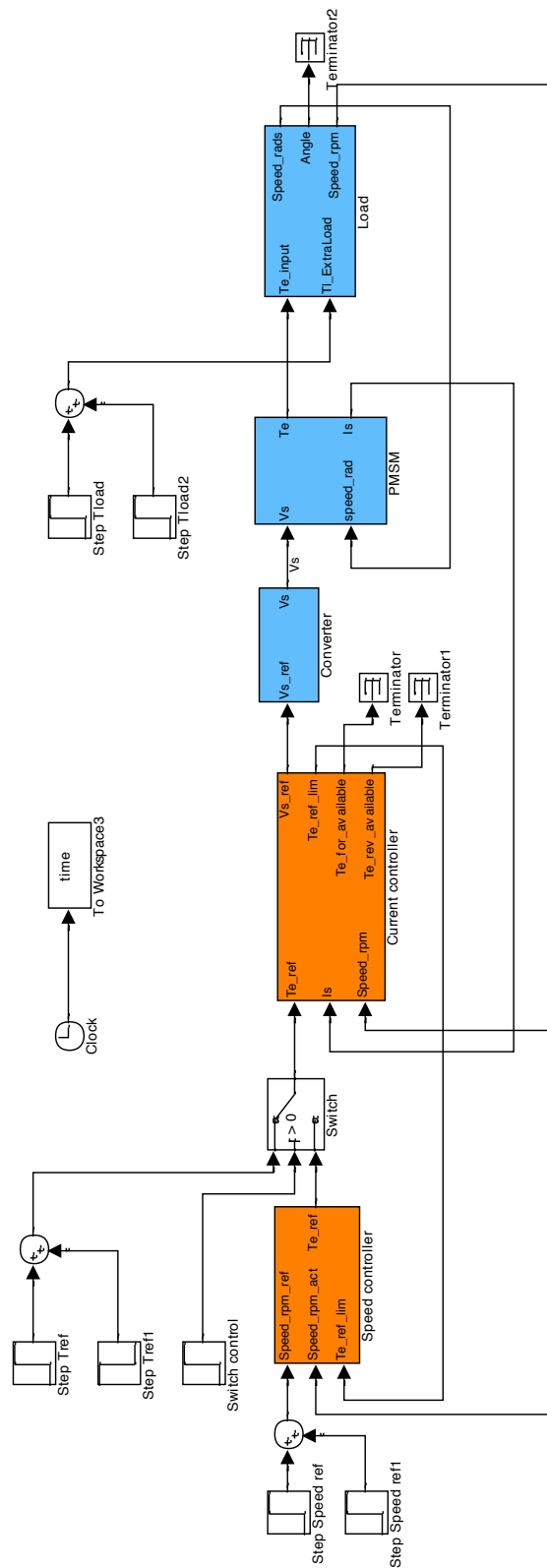


Figure: Overview of simple SUS model

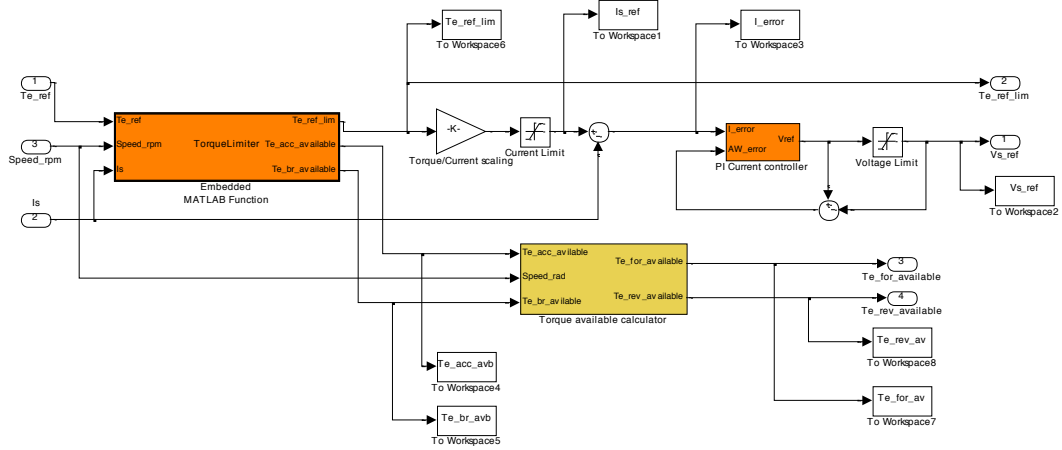


Figure: Current controller in simple SUS model

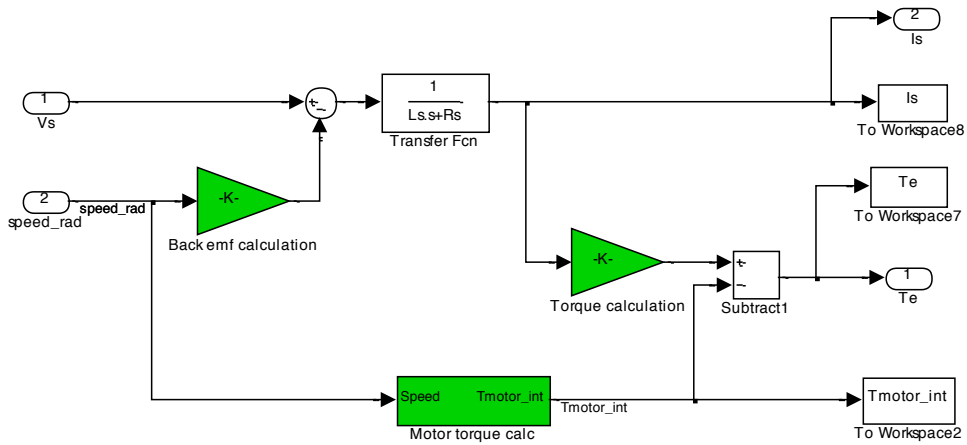
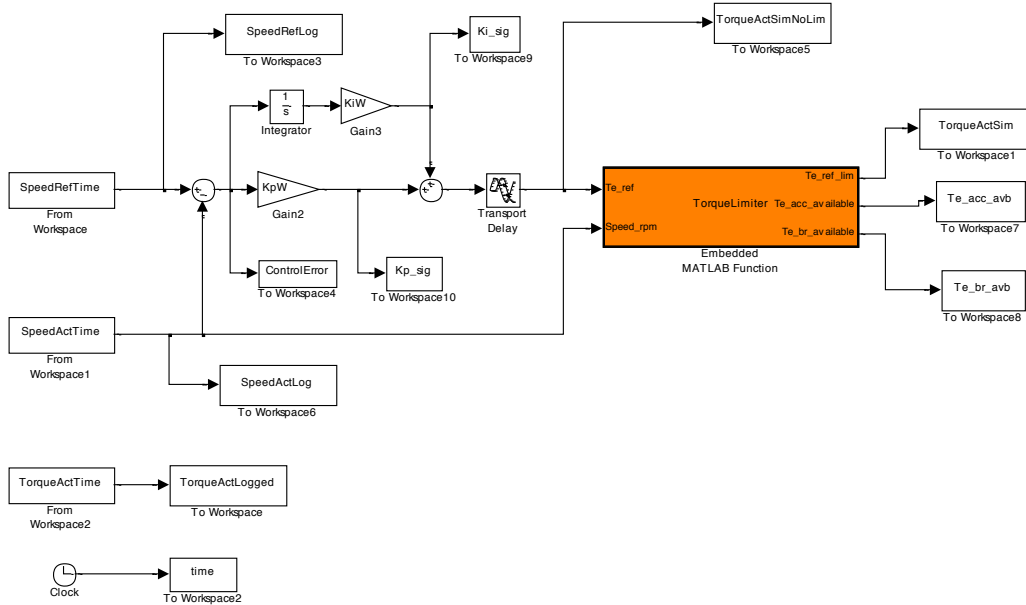


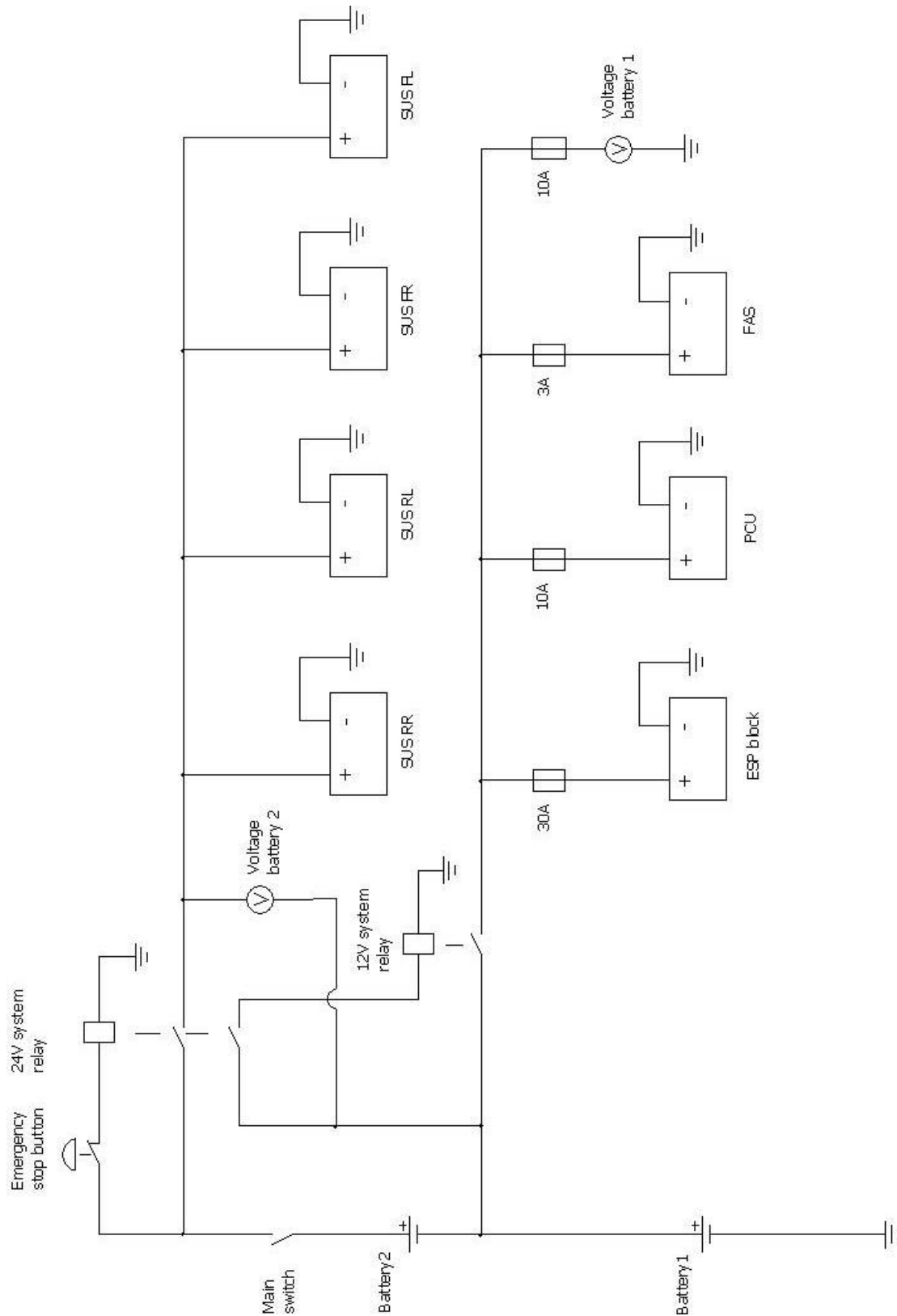
Figure: Electrical parts in simple SUS model

11 Appendix 2: Model used for verification of SUS speed control parameters

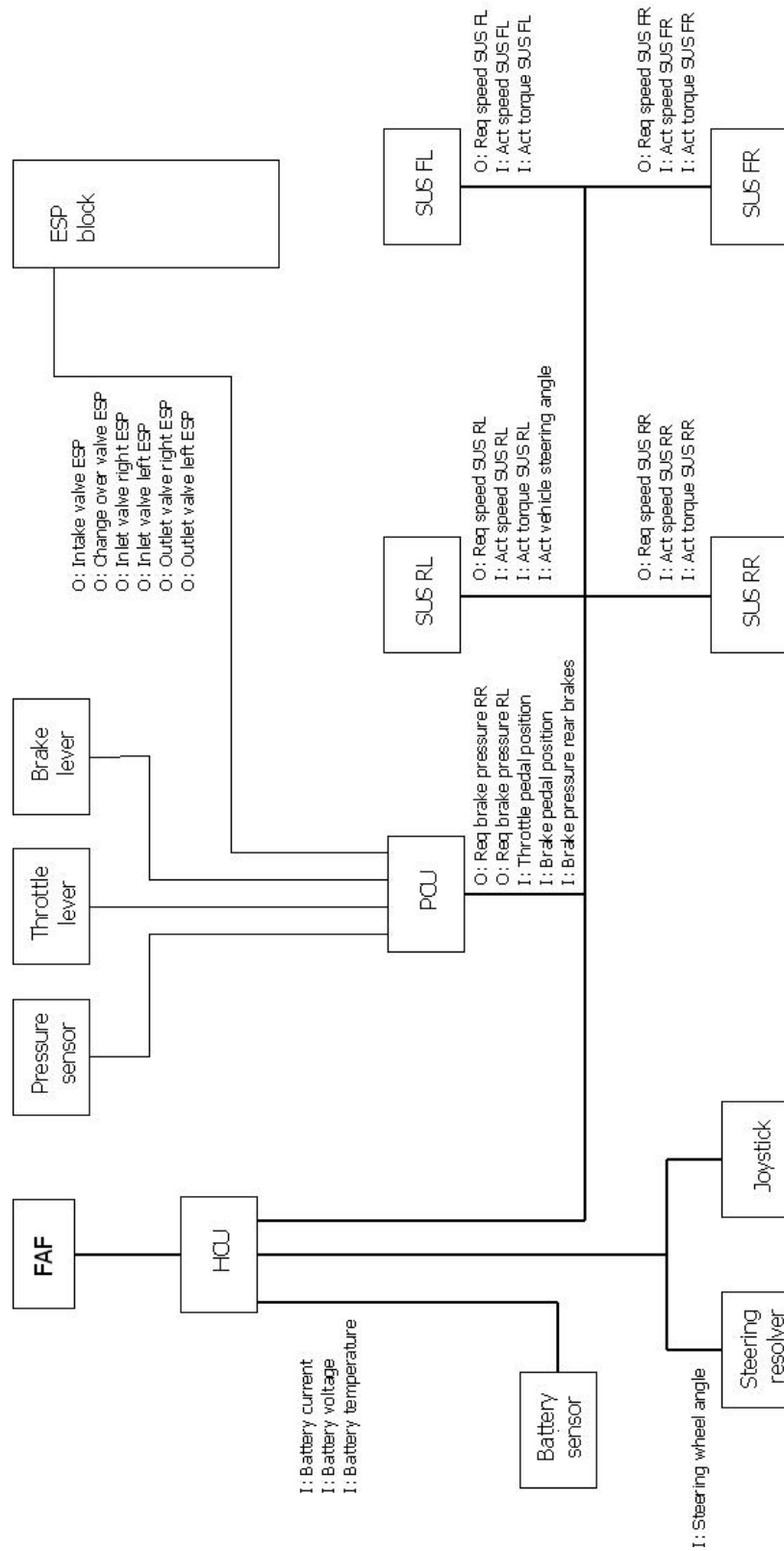
The model below was used for verification of the SUS speed controller parameters. The input to the model is the reference speed to the SUS and output is the simulated torque which can be compared with the logged torque from testing.



12 Appendix 3: Electric power supply schematic for the test platform



13 Appendix 4: Communication and signal overview for the test platform



14 Appendix 5: Test plan and verification of SUS

Revised test plan

Test A-Speed vs torque curve electric motor 1

Outcome: Verification speed vs torque curve, accelerating torque

With the wheels in the air accelerate the SUS to the highest speed that is safe. Then brake it with the mechanical brakes until the speed is zero.

Log: **torque, speed, speed_ref, current**

Test B-Speed vs torque curve electric motor 2

Outcome: Verification speed vs torque curve, accelerating and decelerating torque

With the test platform standing on the ground accelerate the test platform to its highest safe speed and then brake it maximal with electrical braking until the speed is zero.

Log: **torque, speed, speed_ref, current**

Original test plan

Test A-Speed vs torque curve electric motor 1

Test 1: Find the maximum speed for the electric motors (positive and negative)

Log: **torque, speed, speed_ref, current**

Test 2: Make a speed step 0-maxRPMpos(maxRPM in 2 sec)-0

Log: **torque, speed, speed_ref, current**

Test 3: Make a speed step 0-maxRPMpos(maxRPM in 2 sec)- maxRPMneg(maxRPM in 2 sec)-0

Log: **torque, speed, speed_ref, current**

Test setup

Use function: **LMCTR_Send_SUS_Control(UIN8 Tick)** for testing (normal joystick control), change parameter **MAX_THROTTLE** to increase the maximum speed.

Test B-Brake torque static and electric motor damping factor

Outcome: Verify the brake torque and create a basic formula for the brake torque from the pressure and speed. From the zero brake pressure test the damping factor can be calculated.

From the first verification of electric motor speed vs torque curve set possible speed points to test different brake pressures.

Damping factor determination: $T_{brakemotor}(\omega) = B(\omega) * \omega$

Test 1: Set a reference speed, apply a brake pressure and see what torque that is needed from the electric motor to have it running at a steady state speed. Start with not applying any torque so that the torque needed to keep the motor running at no brake torque can be measured.

Log: **torque, speed, speed_ref, current**

Speed (rpm)/Brake pressure	0	TBD	TBD	TBD	TBD	TBD	TBD
500							
1000							
1500							
2000							
2500							
3000							
3500							
4000							
4500							
5000							

Test setup

Use test function: **BrakeBlockTestB**

Test C-Speed vs torque curve el motor 2

Outcome: Verification speed vs torque curve. Find a value for the flux_constant in the motor by using the logged current and torque. $T = 3 * n_p / 2 * \text{flux_constant} * i_q$. Assume all current to be in the q direction.

Test 1: Make a speed step 0-maxRPMpos(maxRPM in 2 sec)-0. Apply a brake torque that is 0,5Nm lower than the electric motor can deliver during the test. (This will give more sample points for the verification curve)

Log: **torque, speed, speed_ref, current**

Test setup

Use test function: **BrakeBlockTestC**, needs brake torque function!

Test D-Brake torque dynamic

Outcome: Verify the dynamic braking performance when changing between different brake torques.

Log: **torque, speed, speed_ref**, current

Test 1: reference speed: TBD; initial brake torque: TBD; final brake torque: TBD

Test 2: reference speed: TBD; initial brake torque: TBD; final brake torque: TBD

Test 3: reference speed: TBD; initial brake torque: TBD; final brake torque: TBD

Test 4: reference speed: TBD; initial brake torque: TBD; final brake torque: TBD

Test 5: reference speed: TBD; initial brake torque: TBD; final brake torque: TBD

Test setup

Use test function: **BrakeBlockTestB**, change the distance between the brake pressure requests to appropriate values.

Test E-Inertia load in the electric motor

Outcome: Determine the inertia in the electric motor.

Test1: Make a speed step and calculate the inertia from this equation: $J \cdot dw/dt = T_e - T_l$.
Function for T_l from the damping coefficient, $T = B(w) \cdot w$. For every time interval calculate dw/dt and T_l and measure T_e . From this the inertia can be calculated.

Log: **torque, speed, speed_ref**, current

Test 1: initial speed: TBD; final speed: TBD

Test 2: initial speed: TBD; final speed: TBD

Test 3: initial speed: TBD; final speed: TBD

Test setup

Use test function: **BrakeBlockTestB**, change the distance between the speed requests to appropriate values.

Test F-How the actual torque follows the reference torque

Outcome: Verify how the actual torque follows the reference torque

Steady state performance:

Test1: Run the lawn mower from the model (FAS). Give throttle and at the same time brake it manually.

Log: **torque, torque_req, current, speed**